# DESIGN OF VIVALDI ANTENNA OPERATING IN TWO FREQUENCY BANDS WITH DISTINCT POLARIZATIONS

A Thesis

by

Mustafa Ayebe

Submitted to the Graduate School of Sciences and Engineering
in Partial Fulfillment of the Requirements for
the Degree of Master's Degree
in the
Department of Electrical and Electronics Engineering

Özyeğin University
July 2022

# DESIGN OF VIVALDI ANTENNA OPERATING IN TWO FREQUENCY BANDS WITH DISTINCT POLARIZATIONS

Approved by:

Asst. Prof. Ahmed H. Akgiray, Advisor
Dept. of Electrical and Electronics Eng.
*Özyeğin University*

Asst. Prof. Hüseyin Şerif Savcı
Dept. of Electrical and Electronics Eng.
*Istanbul Medipol University*

Asst. Prof. Kadir Durak
Dept. of Electrical and Electronics Eng.
*Özyeğin University*

Date Approved: 25 July 2022

# ACKNOWLEDGEMENTS

For the last coupled years, I have had the privilege and honor of working with Asst. Prof. Ahmed Akgiray, my advisor. I have learned so much from his technical knowledge, his humility, generosity, and kindness. I have special thanks to him for always sharing his insight and supporting my scientific endeavors. I am forever indebted to Asst. Prof. Akgiray, a one-of-a-kind mentor and confidant.

To Prof. H. Fatih Ugurdag, I have special thanks to his both before and during my MSc at OzU. I have benefited much from his personal advice.

I would like to thank Mert Karaca for his help to assemble of the dual-polarized Vivaldi antenna.

Obtaining M.Sc. would be so much harder if it were not for the constant support I received from my family, especially my brother Halil Edip. I am deeply indebted to my family who have always supported me, this would be much more difficult without their help.

Last but certainly not the least, I would like to thank my precious parents. To my mother Yeter, thank you for somehow managing to brighten my life. To my wonderful father Hasan, I special thank him for the encouragement and sacrifice during his life.

# ABSTRACT

This thesis presents a novel dual-polarized antenna design based on two orthogonally place Vivaldi antenna elements and are driven by a specially designed feeding network that splits incoming signal into two wherein one of them is linearly polarized between 4 and 6 GHz and the other one is circularly polarized from 14.5 to 15.5 GHz. Splitting of input signal into the two frequency bands, a diplexer is designed. A wilkinson power divider and a transmission-line phase shifter are employed to realize $90^o$ phase difference to achieve circular polarization at the upper frequency band. The feed network is integrated with the Vivaldi elements to ensure a compact form factor critical for reflector applications. In order to avoid crossing of two microstrip-to-slotline transition of the two Vivaldi elements, a small shift between them is introduced. This antenna is intended to be used as a feed antenna for reflector systems employed in radio link systems of drones. Combination of these distinct frequency bands with different polarization requirements allows use of single ground control antenna instead of two independent antennas thereby reducing cost and space requirements.

For demonstration purpose, a prototype is fabricated. The antenna achieves better than -15 dB input reflection coefficients over most of the operating bands and axial ratio is less than 2 dB for the upper frequency range. The antenna exhibits gain between 7.2 to 9.5 dBi from 4 to 16 GHz. Meanwhile, stable radiation patterns are achieved with the cross polarization lower than -25 dB across the operating bands at boresight direction.

# ÖZETÇE

Bu tez çalışmasında, içiçe geçirilmiş iki Vivaldi antenin tasarımı ve anten tarafından gelen/gönderilen sinyali bölüp iki farklı polarizasyon türü ( 4 ile 6 GHz arasinda çizgisel polarizasyon ve 14,5 ile 15,5 GHz aralığında dairesel polarizasyon) elde etmek için özelle tasarlanmış beslenme ağı tasarimi sunulmuştur. Giriş sinyalinin iki frekans bandına bölmek için dipleks kullanıldı. Üst frekans bandında dairesel polarizasyon elde etmek için Wilkinson güç bölücü ve faz dönüştürücü ($90^o$ açı farkını yakalamak için) tasarlandı. Beslenme ağı reflektör uygulamaları için kritik olan kompakt bir form sağlamak amacıyla Vivaldi antenleriyle entegre edilmiştir. Bu anten drone'ların radyo link sistemlerinde kullanılan reflektör sistemleri için besleme anteni olarak kullanılmak üzere tasarlanmıştır. Bu anten farklı frekans bantlarının farklı polarizasyon gereksinimlerinin birleştirilmesi, iki bağımsız anten yerine tek yer kontrol anteninin kullanılmasına izin vermektedir. Bu şekilde maliyet ve alan gereksinimlerini azaltılmış olacaktır.

Bu antenin bir prototip üretilmiştir. Antenin yansıma katsayıları, çalışma bantlarının çoğunda -15 dB'den daha iyi bir sonuç sunmaktadır. Üst frekans aralığı için de eksenel oran 2 dB'den azdır. Anten 4-6 GHz ve 14-16 GHz bantları arasında 7,2 ile 9,5 dBi arasında kazanç sergilemektedir. Bu arada, dar görüş yönünde çalışma bantları boyunca -25 dB'den daha düşük çapraz polarizasyon ile istikrarlı radyasyon desenleri elde edilmektedir.

# CONTENTS

# LIST OF TABLES

# LIST OF FIGURES

# CHAPTER I

# INTRODUCTION

In modern satellite, wireless communication, and radar systems, antennas are required to have the characteristics of both wideband and dual-polarization to satisfy various needs such as expanding the data volume, improving quality of transmitted/received data and increasing the usage bandwidth ratio. Actually, the traditional dual-polarization design requires two separated antennas with individual feeding [1]. However, the space and weight of dual-polarized antenna is twice as much as the single antenna, so that it is inconvenient for actual utilization.

Vivaldi antenna is planar travelling wave antenna with endfire radiation which was first described by Gibson in 1979 [2]. Vivaldi antenna consists of a feed line and radiator, and usualy Microstrip/slotline transition is used for feeding mechanism. Radiator is usually exponentially tapered, however, examples of linear, parabolic, hyperbolic or polynomial curves can be found in [3].

The Vivaldi antenna is widely studied to fulfill different application requirements and due to its wide-band application, low cost, simple structure and relative insensitivity to dimensional tolerances in fabrication processes. Various linearly polarized (LP) Vivaldi antennas have been published for gain or directivity enhancement [4, 5], ultra-wide operational bandwidth [6, 7], dual-polarization application [1, 8, 9]. Due to its inherent advantage, wide operational bandwidth and high gain circularly polarized (CP) antenna by using the Vivaldi antenna structure is developed [10].

## *1.1 State-of-the-art in Vivaldi Antennas*

As alluded to earlier, the Vivaldi antennas are the standard bearer in terms of reflector feed antenna for wideband applications. They can meet or exceed all the requirements of the reflector systems, namely;

1. low sidelobes
2. good cross-polarization
3. constant or near constant phase center with operating frequency bands
4. symmetric radiation pattern

Due to increasing interest of wide-bandwidth applications, there has been much points in feed antennas accomplished large bands in the last a few years. As a result of wideband feed antennas with LP, dual LP, and CP have been offered.

The most common way to employ two orthogonal polarization with Vivaldi antennas is to place them orthogonally and fed them properly [1, 9, 11, 12]. These studies present a wide bandwidth dual polarized Vivaldi antenna. Their goal was to find an economical antenna model with good antenna features over the operating frequency band.

In [10], a new Vivaldi antenna with wide operational bandwidth and CP radiation is proposed as presented in Figure 1. With this design, 3 dB axial ratio and impedance bandwidth are between 2.35 to 7.18 GHz. Beside that, the radiation patterns are symmetrical and stable in the operating band. The feeding structure is integrated on the Vivaldi antenna, to make full use of the antenna space as shown in Figure 1.

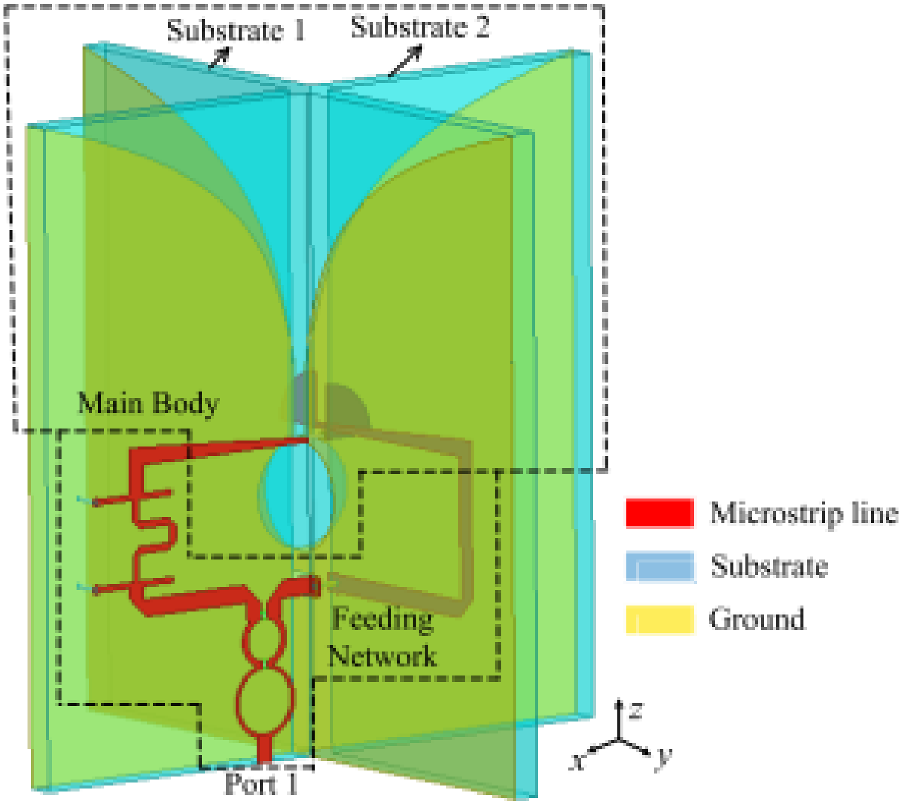


**Figure 1:** Circularly polarized Vivaldi antenna

Studied to orthogonally located dual-LP Vivaldi antenna structures shown in [1, 9, 11, 12] and CP Vivaldi antenna presented in [10], the proposed dual-polarized antenna structure in this communication offers linear polarized operation at C-, and circular polarization at K- bands. The proposed antenna structure has better impedance matching compare to [1, 9, 11, 12] in the operating bands. The isolation performance of the feeding ports operates less than -25 dB. For the analogy, the cross-placed Vivaldi antennas offered in [9, 11, 12] and [10] achieve port-to-port isolation between -15 and -25 dB.

Referring to the CP Vivaldi antenna in [10], a novel cross-placed Vivaldi antenna with specially designed feed network which operates with linear polarization from 4 to 6 GHz and circular polarization in 14.5 to 15.5 GHz bands is proposed in this thesis.

This antenna is intended to be used as a feed antenna for reflector systems employed in radio link systems of drones. Combination of these distinct frequency bands with different polarization requirements allows use of single ground control antenna instead of two independent antennas thereby reducing cost and space requirements.

## 1.2 Outline of the Thesis

This thesis have been divided into four parts with starting introduction, motivation and background of this work followed by short description of state of the art. Then, design and analysis of the antenna structure based on the radiating structure of the Vivaldi elements, feed mechanism and feed network is dedicated on second chapter.

Third part of this work describes the final simulations of the proposed Vivaldi antenna. Example prototype is fabricated and measured. Then, the comparison with the simulations and measurements have been presented.

In the last chapter, our study is concluded with comments on the design of Vivaldi antenna operating in two frequency bands with different polarizations.

## 1.3 Publication

- Mustafa Ayebe and Ahmed H. Akgiray, ”Design of Dual-Polarized Vivaldi Antenna”, *submitted to IEEE International Symposium on Antennas and Propagation and USNC-URSI Radio Science Meeting (APS/URSI)*, July 2022.

# CHAPTER II

# DESIGN AND ANALYSIS OF PROPOSED ANTENNA

The two Vivaldi antennas are located orthogonally and are driven by a novel designed feeding structure which splits incoming signals into two wherein one of them is linearly polarized in 4 - 6 GHz and the other one is circularly polarized in 14.5 - 15.5 GHz bands, and ensure good radiation performance. In order to divide the input signal of antenna into two-way signals for C-, and Ku- bands, diplexer [13] is used. The diplexer comprises a stepped-impedance low-pass filter (LPF) [14] and an edge-coupled bandpass filter (BPF) [15]. A Wilkinson power divider (WPD) [13] and a transmission-line phase shifter are employed to compensate $90^o$ phase difference to achieve CP at the upper frequency range. The proposed dual-polarized antenna is employed by joining the radiators and feed network properly. With this motivation, the main structure of our antenna is presented in Figure 2.

## *2.1 Radiating Structure*

In this part, radiators are investigated starting with overview and followed by short description of curvature profiles. Then, the qualitative look of radiating elements is offered.

### 2.1.1 Overview of Vivaldi Antenna

Basically, Vivaldi antenna is a planar antenna which operates in wide-band region with linear polarization. As shown in Figure 3, to the left of the cavity is a short circuit and this operates like a parallel inductor. The right side of the cavity is the radiating section. It can be regarded a tapered slot Vivaldi (TSV) antenna which is proposed by Gibson in 1979 [2].

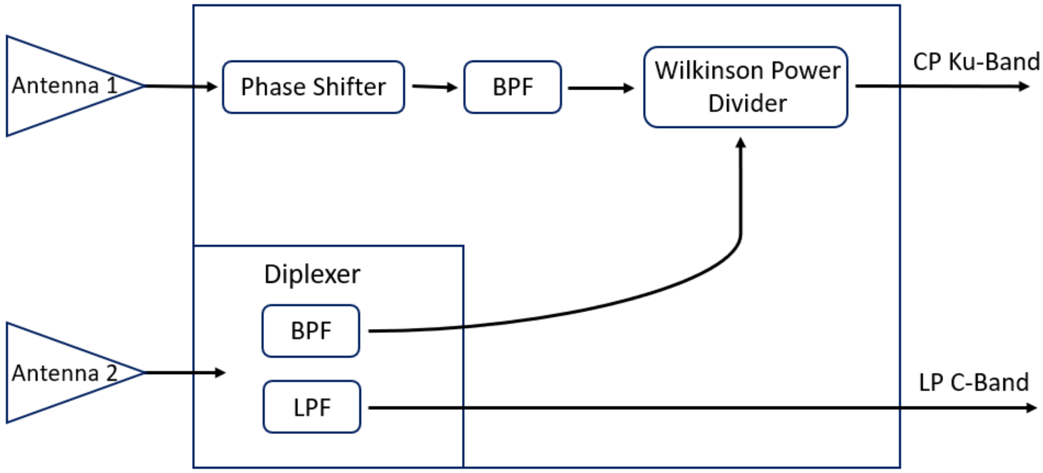


**Figure 2:** Proposed Antenna Structure

This model introduces two limits for the operating frequency range of the antenna. Tapered opening of the antenna should be greater than one-half of the wavelength,

$$w_{opening} \geq \frac{\lambda_0}{2} \tag{1}$$

where $w_s$ is width of the slot, so as to achieve the desired raditation performance [16]. Therefore, width of the antenna approximately defines the lowest frequency cutoff, while width of slotline is introducing the high frequency which is radiated by the structure [17].

Slotline is a balanced transmission line, thus a balun is required to transform to a single-ended transmission line. Creating a wideband balun to feed the radiating structure is usually complicated task, applying this solution is somewhat inconvenient [18]. Therefore, microstrip feed line to slotline transition, as shown in Figure 3, is mostly used in TSV antennas. This transition defines the matching, gain, and radiation performance. It is possible to offer a flowing which works over the wide frequency range.

Thin substrates with low values can cause radiation and matching problems. An optimal range of effective dielectric thickness to the free space wavelength ($\lambda_0$) ratio

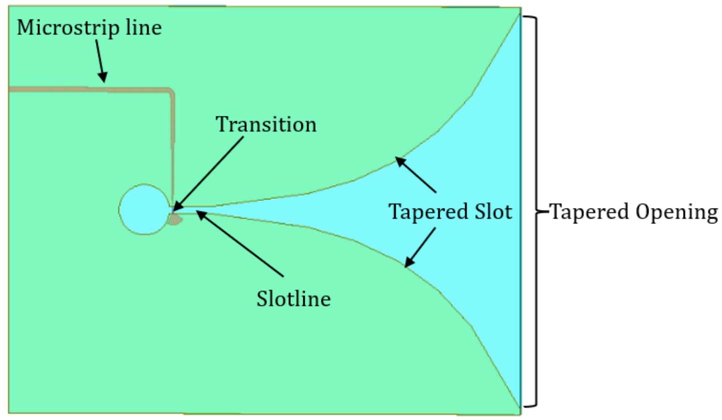


**Figure 3:** Tapered Slot Vivaldi Antenna

has been determined about 0.005 and 0.03, and the effective dielectric thickness is introduced by

$$h_{s_{eff}} = (\sqrt{\epsilon_r} - 1)h_s \tag{2}$$

where $h_s$ is substrate thickness and this rule holds for any Vivaldi structure between $4\lambda_0$ to $10\lambda_0$ long [19]. Similarly, in [16], empirical rules were improved for both optimum structures and long structures.

Many changes on the original Vivaldi had been presented to develop the antenna structure features. [20] illustrates trials to enhance both the H and E plane pattern and to achieve low side back lobes by presenting configurations on the antenna exterior sides. The other developments deal with the operating frequency band constrains by altering geometry of the curvature profiles [16].

### 2.1.2 Curvature Profile

While there are many parameters to define the Vivaldi antenna geometry, designing a Vivaldi antenna with a prescribed beamwidth reduces to proper selection of the taper curvature. The flare profile can be linear, polynomial, hyperbolic, or exponentially curved etc. The optimal taper profile combination is the one that achieves:

**Table 1:** Curvature profiles

| Profile Name | Expression |
|---|---|
| Linear | $y = y_i + (y_f - y_i)\frac{x}{L}$ |
| $x^r$ | $y = y_i + (y_f - y_i)\left[(1-s)\frac{x}{L} + s\left(\frac{x}{L}\right)^r\right]$ |
| Hyperbolic | $y = \sqrt{y_i^2 + \frac{x^2(y_o^2 - y_i^2)}{L^2}}$ |
| Polynomial | $y = y_i + (r+1)(y_o - y_i)\left(1 - \frac{rx}{(r+1)L}\right)\left(\frac{x}{L}\right)^r$ |
| Exponential | $y = c_1 e^{Rx} + c_2$<br>$c_1 = \frac{y_f - y_i}{e^{Rx_f} - e^{Rx_i}}, \quad c_2 = \frac{y_i e^{Rx_f} - y_f e^{Rx_i}}{e^{Rx_f} - e^{Rx_i}}$ |

1. Wideband application,

2. Symmetric radiation pattern with a prescribed nominal beamwidth.

3. Little or no change in radiation patterns with the operating band.

4. Smooth impedance transformation 110 Ω to free-space impedance.

Profile options considered in this study. All profiles except the exponential are from [21]; the exponential curve is a modified version of [22]. $(x_i, y_i)$, $(x_f, y_f)$ are peak and bottom point of tapered curve, respectively;$L$ is the taper length; $r$ is the exponent of polynomial; $R$ is the exponential factor and $c_1$ and $c_2$ are constants; $s$ is a parameter between $[0, 1]$ that determines how much linear taper is added.

While majority of the prior work on Vivaldi antenna focuses on exponential profile for optimal radiation performance [16, 20, 22], many other profiles have been investigated in this research, most of which are from corrugated and smooth-taper literature [21]. Expressions for all the profiles used in this work and their plots for a typical taper are presented in Table 1 and Figure 4, respectively

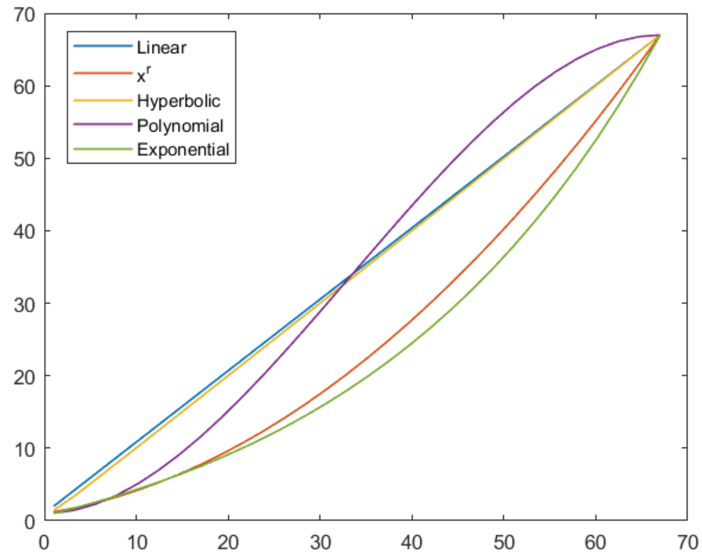


**Figure 4:** Taper Profiles

### 2.1.3 Qualitative Look: Radiating Elements

While there are many parameters defining the antenna geometry, designing a TVS antenna with a prescribed beamwidth reduces to proper selection of the taper profile. The optimal profile combination is the exponential curvature for this work.

3-D view of the proposed dual-polarized antenna's radiating structure is shown in Figure 5. The two elements are orthogonally placed and they are almost identical except the position of microstrip-to-slotline transition of each elements. The small shift on vertical axes is introduced to avoid feed lines overlapping at the crossing point. This introduced shift is also studied in feed mechanism design and proposed solution.

Figure 6 shows the detailed model of each antenna elements. The flared slotline, open-ended slotline with circular cavity, microstrip/slotline transition, and open-ended microstrip line with stub ($R_{cavity}$, $R_{stub}$, $w_0$, $l_f$) are used to improve the antenna matching performance and employ the exponentially TVS antenna effectively. The

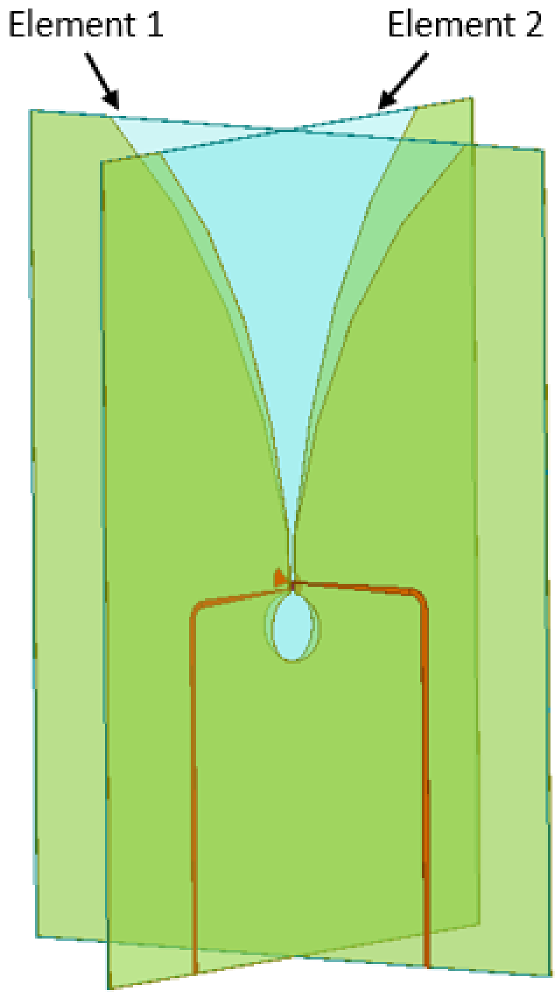


**Figure 5:** Perspective view of the radiators

feed line along the horizontal axes is inroduced as

$$f_{line} = w_0 + (w_f - w_0)\frac{x}{l_f} \tag{3}$$

Impedance transformation 110 Ω to 50 Ω impedance can be achieved for wideband application. The parameters of $R_{cavity}$, $R_{stub}$, and $w_0$ are set fairly to employ smooth microstrip-to-slotline transition.

As shown in Figure 6 (a), a slot with the width of $h_{stbu}$ is cutted off at the center line of the antenna along the lower part. Also, the same procedure is made on second element, but in this case there is a cut at the upper part antenna which is given in

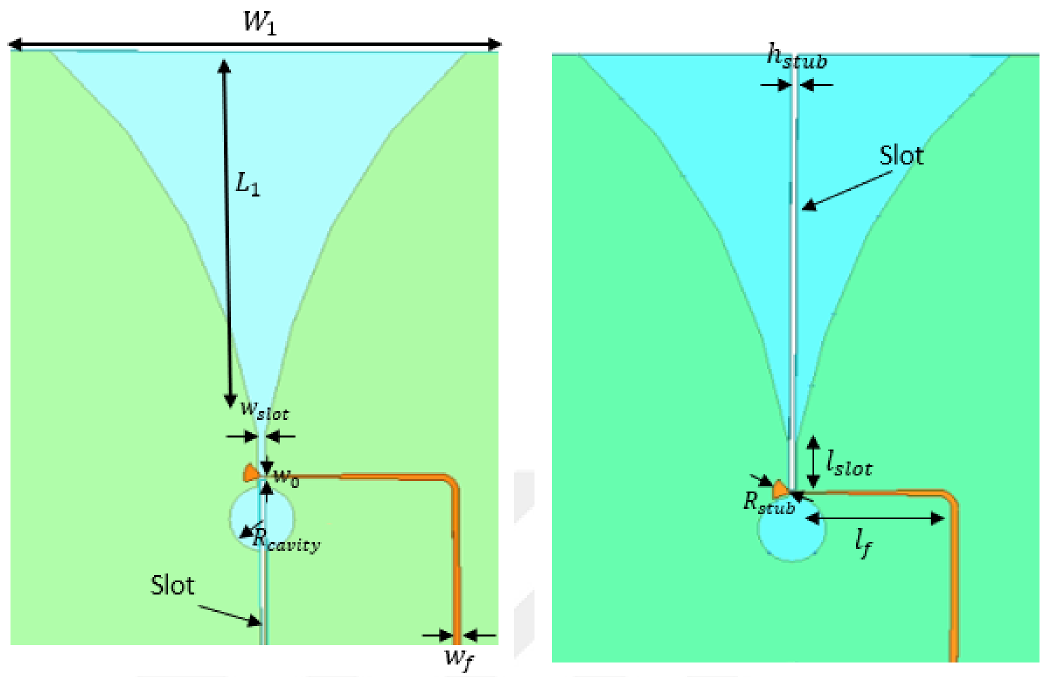


(a) (b)

**Figure 6:** Radiating structure of two antenna (a) front perspective of 1. element; (b) front perspective of 2. element

Figure 6 (b).

As discussed, the antenna width and length should be greater than one-half wavelength and a wavelength at the lowest frequency, respectively. This need ensure fair gain, wide-band matching and radiation pattern performance. The wavelength of minimum operating frequency is $\lambda_l = 75mm$ ($f_{min} = 4GHz$)for our work. Thus, width of antenna $W_1 \geq 37.5mm$ and $L_{antenna} \geq 75mm$ will provide reasonable radiation pattern performance.

$W_1$ and antenna length ($L_1 + l_{slot} + 2R_{cavity} + backwall$) is taken 100 and 132 mm, respectively for the optimal results of the gain, return loss at operating bands, and radiation performance

To observe the performance of each Vivaldi antennas, simulation results are presented for both antennas separately (which are shown in Figure 6). The reflection coefficients of each element are presented in Figure 7, and it can be seen that the

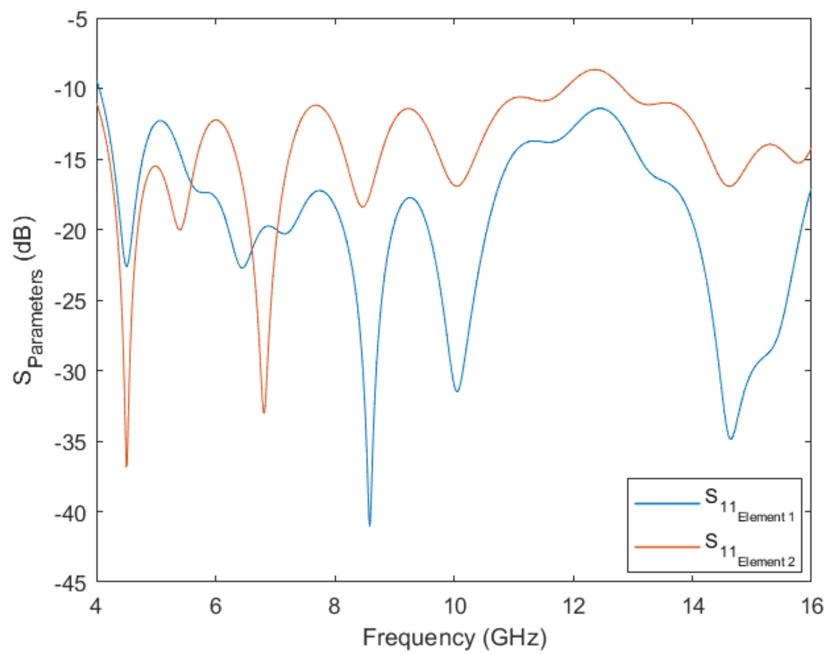


**Figure 7:** Simulated reflection coefficients of the element 1 and element 2

antenna 1 has -20 dB for upper frequency range and antenna 2 performs less than -13 db over much of both frequency bands.

Figure 8 presents the simulated radiation patterns of the element 1 and element 2 at 4 GHz, 5 GHz, 6 GHz, 14 GHz, 15 GHz, and 16 GHz at E-plane. As observed that simulated radiation patterns of each antenna are symmetrical in the operating bands. The performance of side/back lobes are also reasonably good.

The realized gain of the each antenna exhibits gain between 7.2 to 9.9 dBi for the both operating frequency bands. The simulated efficiency is better than 0.9 in pass-band in C- and Ku- bands.

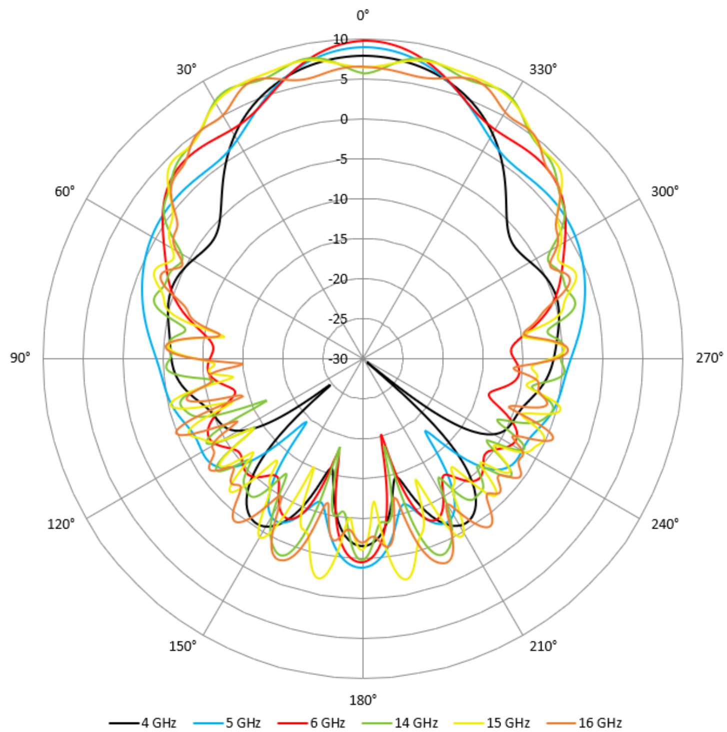


(a)

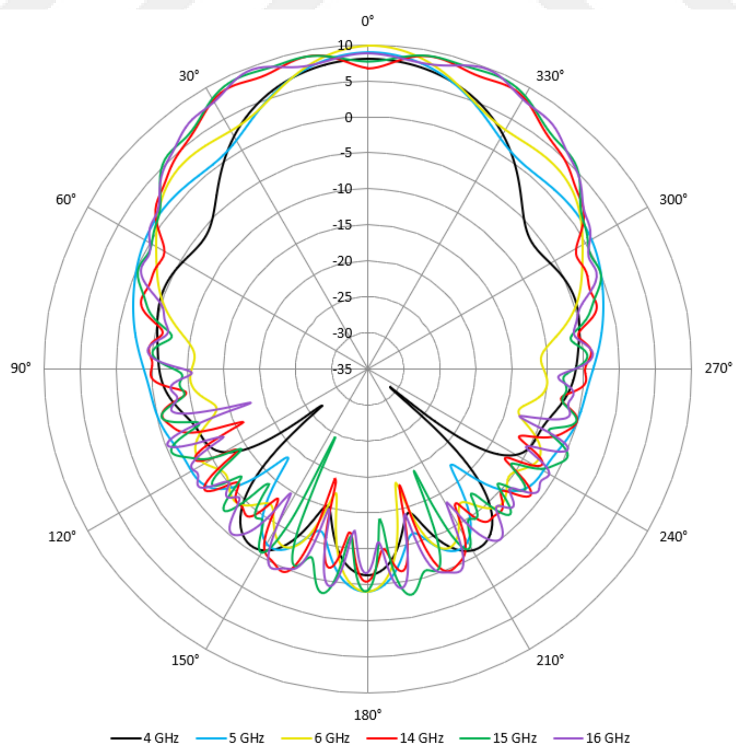


(b)

**Figure 8:** Simulated radiation pattern of the (a) Element 1; (b) Element 2 at different frequencies

## 2.2 The Feeding Mechanism Approach

The TSV antenna is most effective with a slotline flares. Thus, a transition is designed to coupled signals to the slotline taper of Vivaldi from the free-space. There is low loss for transition over a operating wide bandwidth and compact and easy to fabricate.

In [23], the basic slotline to microstrip line transition is met at $90^o$ angle. Microstrip line is ended by a stub, and this stub produces a virtual short at the transition point, virtually shunting the microstrip-to-slotline flares. This facilitates the traveling region to pair into the slotline on the opposite metal layer. The slotline is also terminated by cavity which is used to prevent the back radiation. The field can propagate without any reflection and insertion losses through the slotline to microstrip transition.

### 2.2.1 Equivalent Circuit for Microstrip/Slotline Transition

The TSV antenna is a equivalent antenna model. Thus, the structure requires the feeding point to receive or transmit the EM waves fairly over the TSV antenna. The most common feeding structure used with TSV antennas is Knorr's slotline-to-microstrip line transition [24].

To study the feautures of the optimal microstrip/slotline transition over the operating frequency region, the equivalent feeding network is divided into two sections as shown in Figure 9. These are (a) cavity and (b) a link of stub and cavity illustrating the microstrip/slotline transition of the offered Vivaldi antenna model [1].

In Figure 9, $R_{cavity}$ and $R_{stub}$ are the radius of the cavity and stub, respectively, while $Z_{L1}$ and $Z_{L2}$ are the loads to match the transition point impedance of Vivaldi feeding to the free space impedance. In our research, $Z_{L1} = Z_{L2} = 110\ \Omega$, which is the average our input impedance of the isolated Vivaldi antennas fed by a slot transmission line over the operating frequency bands (from 4 to 6 GHz and 14 to 16 GHz).

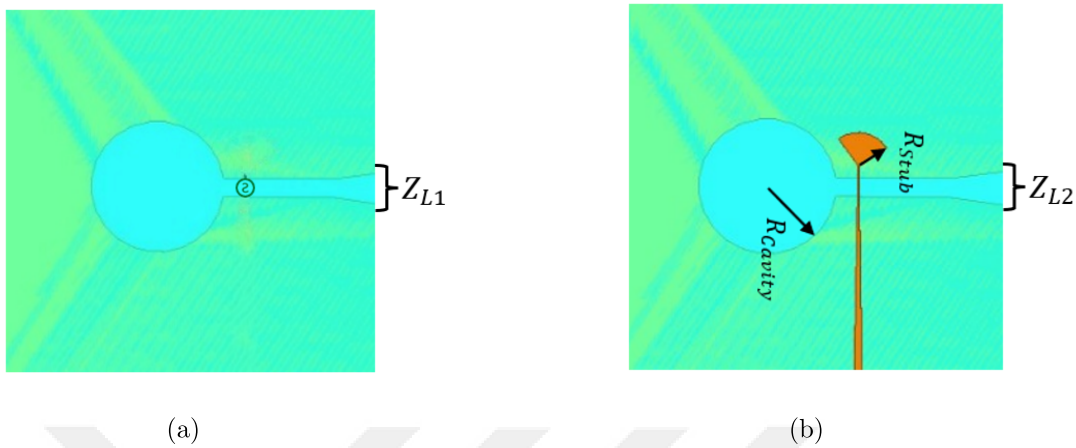


**Figure 9:** Balanced circuit: (a) only cavity; (b) link of stub and cavity to present the microstrip-to-slotline transition

The balanced circuit of Figure 9 (a) have been simulated for $R_{cavity}$ is between 2 and 9 mm. Figure 10 depicts the simulation results of the cavity. As observed, When $R_{cavity}$ goes up, the input real part impedance has more fluctuations at the lower frequency bands, but as the frequency and radius increases, the fluctuation becomes more stable. In this thesis, regarding the desired impedance of the cavity, the optimal value for cavity radius is found by optimization as $R_{cavity} = 5.44mm$.

The input real part impedance mainly shows the feature of the cavity. However, the imaginary part of input impedance, especially with the bigger cavity, are resulted as complementary proposing impedance stable fluctuation around zero, [1].

The results show that cavity radius (5.44 mm) with a stub 2.88 mm radius offers the best impedance matching and gain performance over the desired frequency range.

### 2.2.2 The Radial Stub Position

The stub placement can be presented in 2 ways: vertical and horizontal dislocation which has been depicted in Figure 11.

If the feed stub is placed along the antenna's axis, its location position is introduced as vertical replacement. It's defined by $L_{off}$. The zero location of $L_{off}$ is

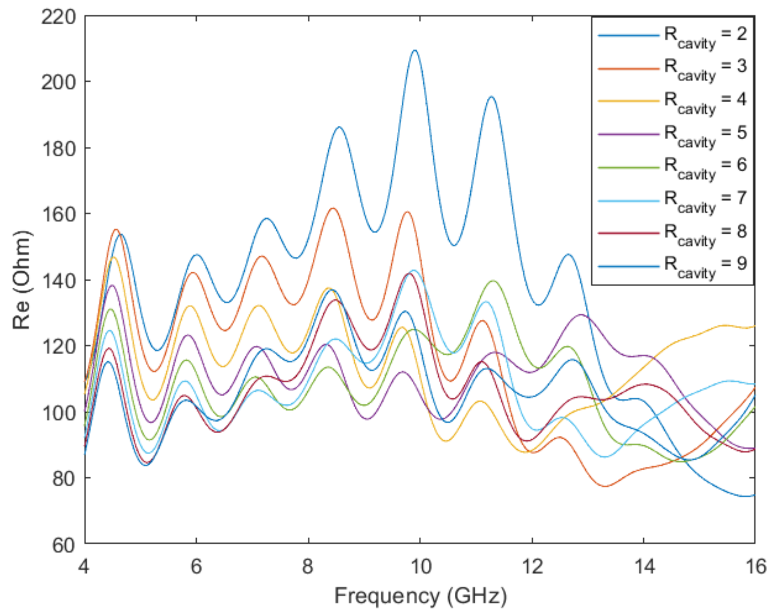


**Figure 10:** Simulated real part of the input impedance of cavity with different $R_{cavity}$

specified as the intersection point of the cavity and slotline. If our stub moves through the antenna's width, its position is introduced as horizontal replacement. It's defined by $W_{off}$.

The taper slot width changes with respect to stub's vertical placement in the antenna's axis where it meets with the microstrip feed. Hence if the slotline impedance changes, it affects the transition of the microstrip-to-slotline [25]. It inevitably change antenna's impedance and affect the matching performance over the operating frequency bands.

The changes the length of microstrip line also alters the matching performance because line impedance transformation performance alters as the line's length changes. The feed line linear transformation is given by Equation 3. Length of microstrip line and taper slot width are more critical at higher frequencies. The vertical position of stub, ergo, $L_{Off}$'s value defines $f_{High}$ and $f_{Low}$ in an optimum maner

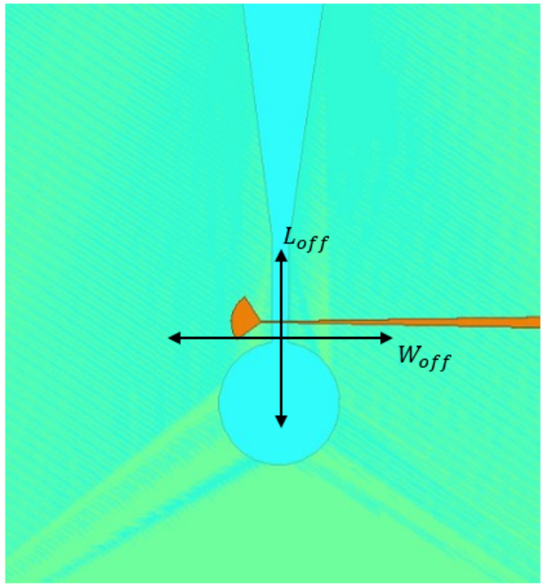


**Figure 11:** Dislocation of the radial stub

Stub's dislocation on horizontal position are very important parameter in the antenna's frequencies applications. This parameter changes the terminal line impedance value in the sample feed line wavelength at each frequencies. In [25], observing $f_{Low}$ specification, one recognises that it includes slight changes as compared with $f_{High}$ diagram.

As $L_{off}$ and $W_{off}$ parameters alter, $f_{Low}$ and $f_{High}$ values also change, ergo, both parameters are regarded simultaneously to make flowing usage of $L_{off}$ and $W_{off}$ parameters to adjust the frequency limitation of the antennas.

The presented analysis proposes a proper system to construct a broadband equivalent circuit for microstrip/slotline transition and offers the designer a basic mechanism to modify the antenna model between its feeding point and free space [23]. While, the input impedance of the microstrip feed antenna requires to be designed based on stub angle too, and this analysis will not be considered.

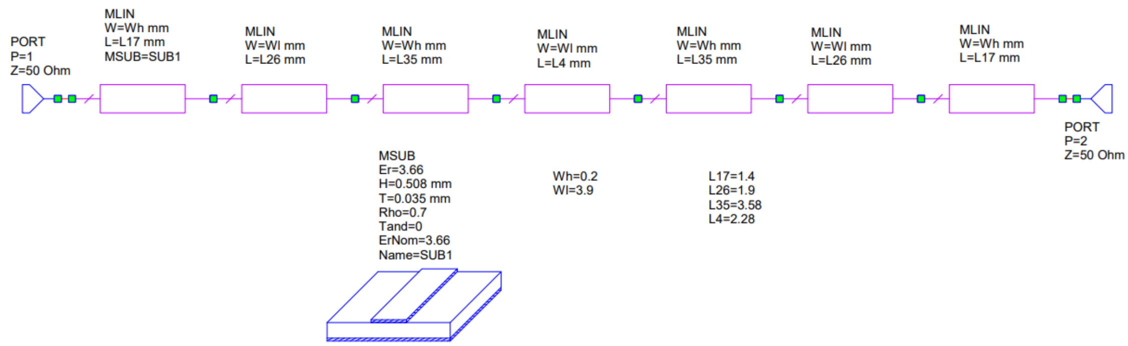


**Figure 12:** Schematic of Stepped-Impedance Lowpass Filter

## 2.3 *Feed Network*

To realize the linear and circular polarization, and guarantee a good impedance matching and radiation performance, the feeding network is specially designed. In order to divide the incoming signal of antenna into two-way signals for C-, and Ku-bands, diplexer is used. The diplexer comprises a stepped-impedance low-pass filter and an edge-coupled bandpass filter. A wilkinson power divider and a transmission-line phase shifter are employed to realize $90^o$ phase difference to achieve circular polarization at the upper frequency band.

### 2.3.1 Diplexer with LPF and BPF

In this section, feed network is introduced which is the combination of diplexer with stepped-impedance LPF and edge-coupled BPF, Wilkinson power divider, and transmission line phase shifter on AWR Microwave Office [26]. Firstly, diplexer design study is focused. It's known that diplexer is three-port device that sorts the input signal out to two way channels, dependent on frequency [13]. The incoming signals must be offset in frequency band by an appreciable rate so that filter can do their job to split them. Our diplexer can be used low-pass and band-pass filter to achieve the desired result. As given [14], typically maximally flat stepped imppedance low pass

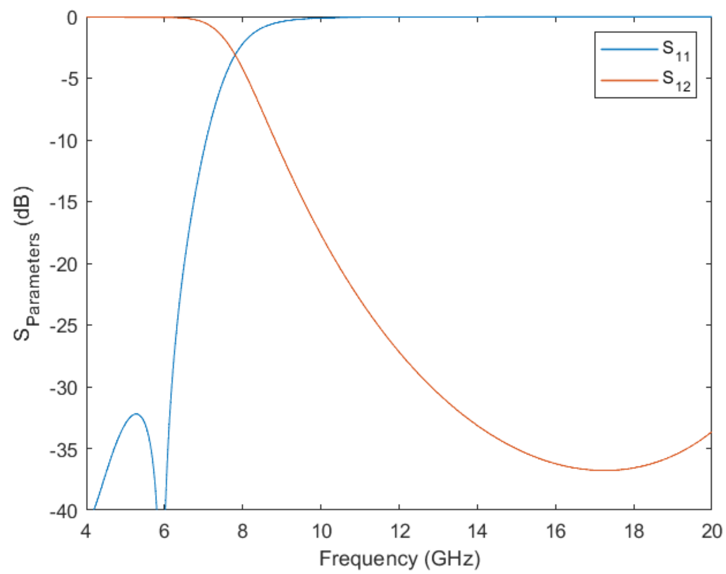


**Figure 13:** S-parameters of stepped-impedance low-pass filter

microwave is first designed filter for N=7 (schematic is given in Figure 12) with a 7.8 GHz cut off frequency, the value of insertion loss is -20 dB at 11 GHz, and the return loss is better than -30 dB for operational band as shown in Figure 13.

Design of the edge-coupled bandpass filter which is presented in Figure 14 is based on $\lambda/4$ resonators, i.e. the length of all the microstrip lines are equal to $\lambda/4$ [15]. Wizards tool is used to design the BPF at Ku band.

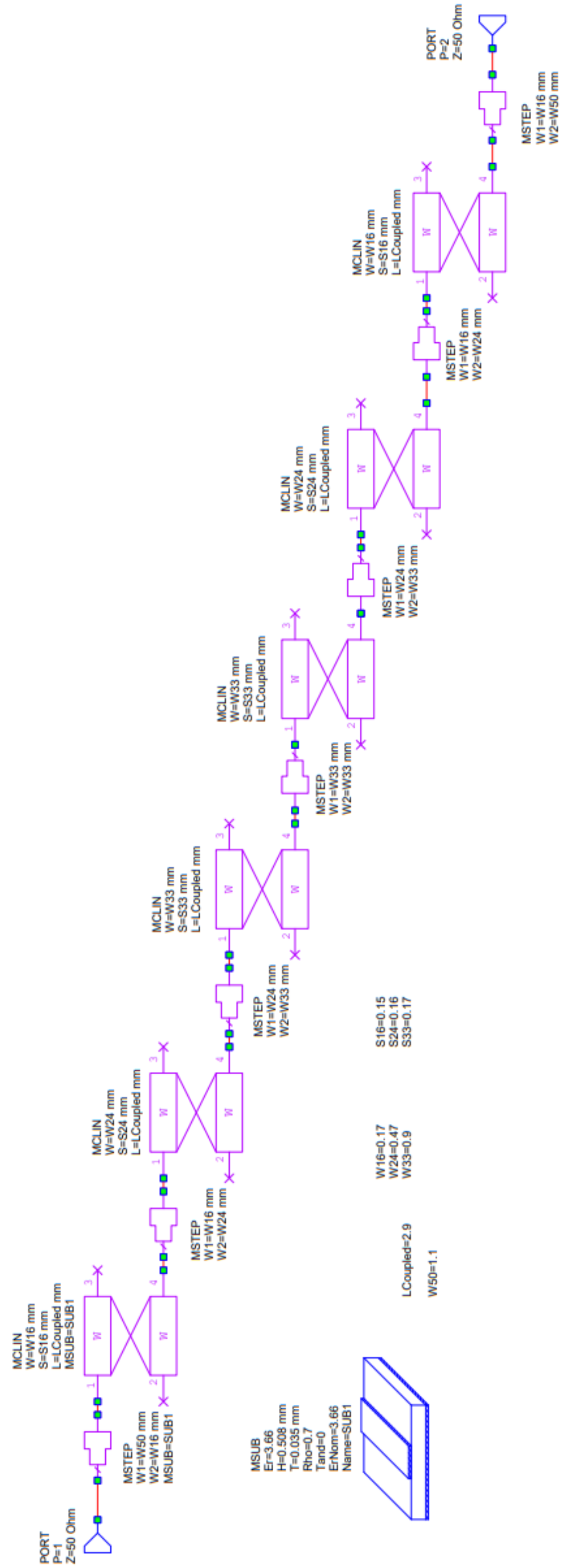


**Figure 14:** Schematic of Edge-Coupled Bandpass Filter

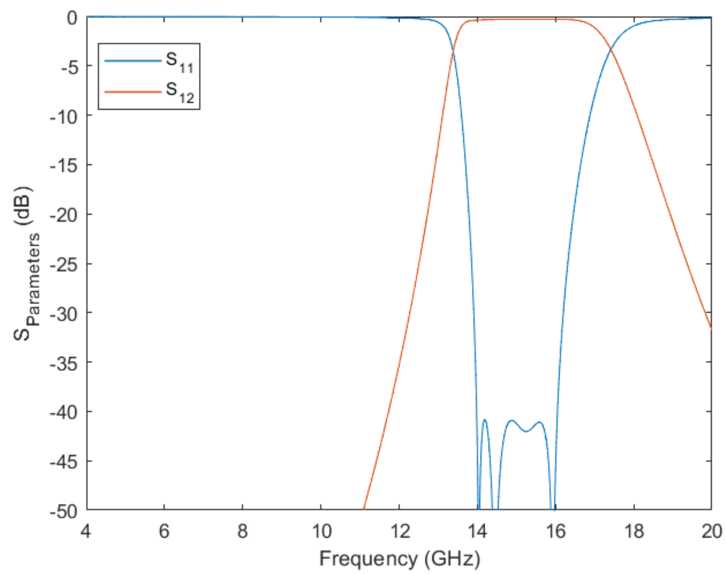


**Figure 15:** S-parameters of edge-coupled bandpass filter

Based on design specifications, BPF is proposed with $6^{th}$ order, pass band ripple 0.1 dB, and return loss is less than -40 dB for upper frequency band operation as evidenced in Figure 15.

Now, diplexer can be proposed. The individual channels of the diplexer are described by LPF and BPF equaivalent circuits. Two filters are joined together with using two transmission lines to a common junction. The each transmission line rotates the each response of filter to open circuit in the passband of the other filter. This is the simpliest way to design a diplexer and our schematic of diplexer is shown by Figure 17.

The transmission and reflection coefficients are given in Figure of 18. There is almost no insertion loss as evidenced in Figure 18 (a). The input reflection coefficients are better than -10 dB over the operating bands (shown in Figure 18 (b)). With given results, good starting point is achieved for combination of the diplexer and the other parts of the feed network.

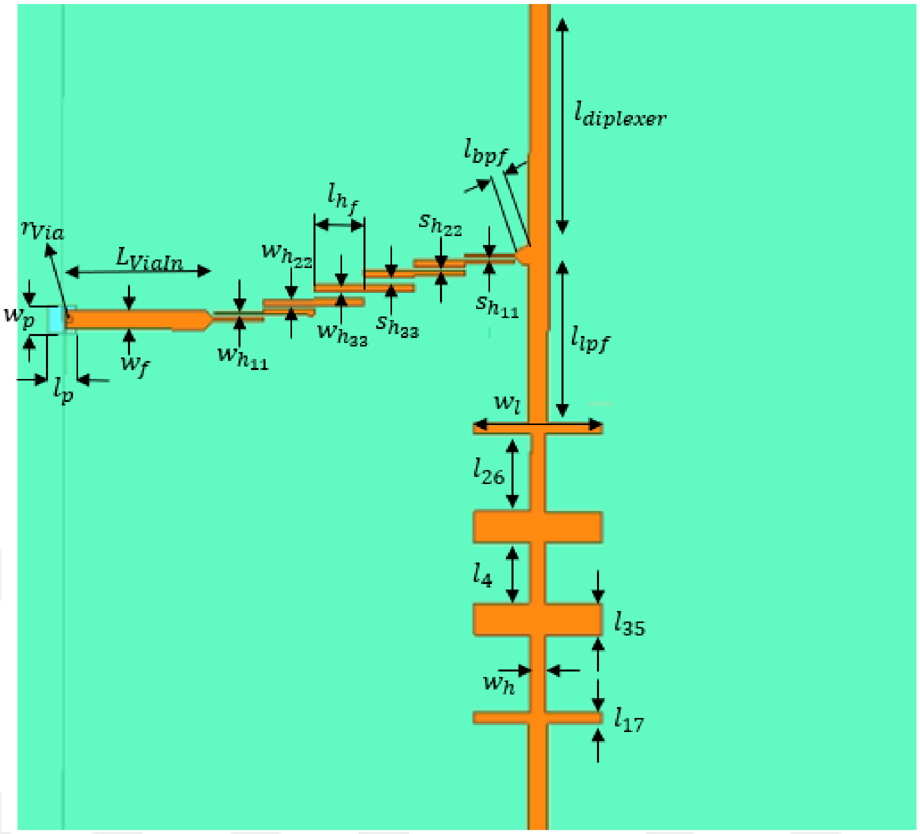


**Figure 16:** Diplexer with LPF and BPF

Figure 16 which is taken from electromagnetic simulator presents a close-up of the diplexer the combination of stepped impedance LPF and edge-coupled BPF. Also, the metalized via is used to connect the microstrip trace of Wilkinson power divider on orthogonal element, as shown in Figure 16. The only used are is shown for clarification.

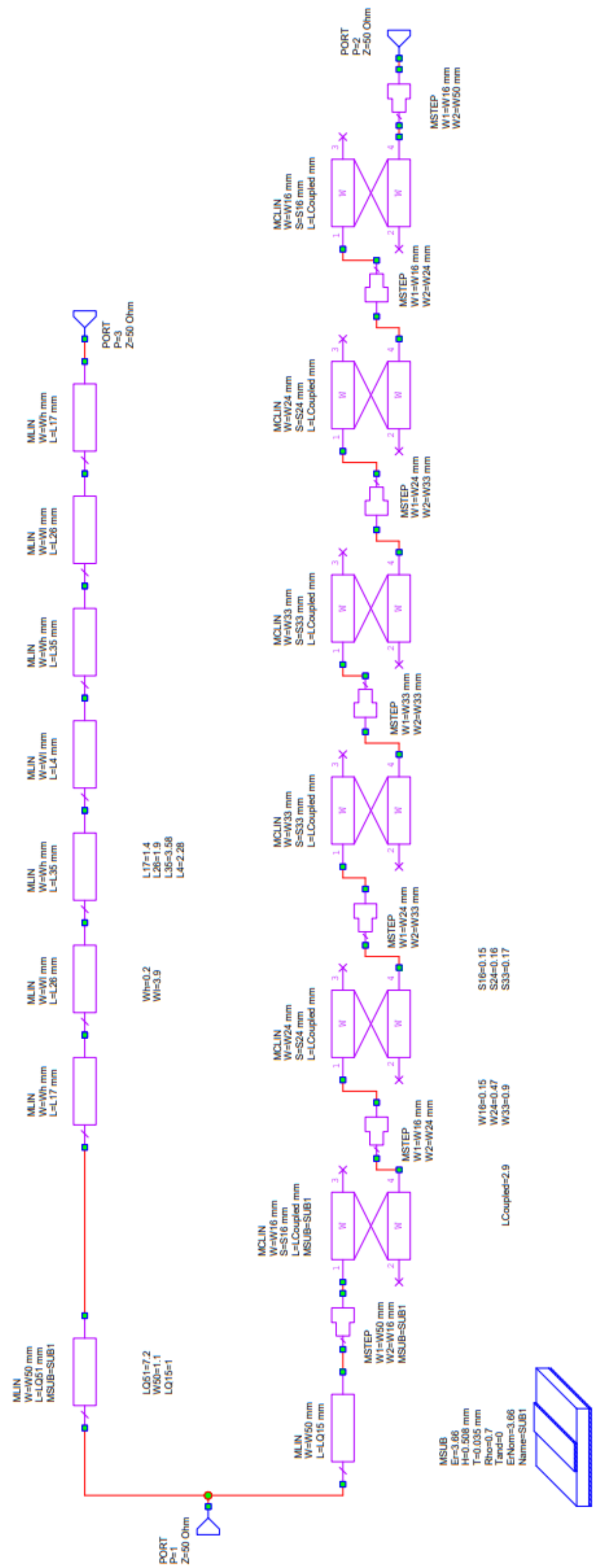

**Figure 17:** Schematic of diplexer

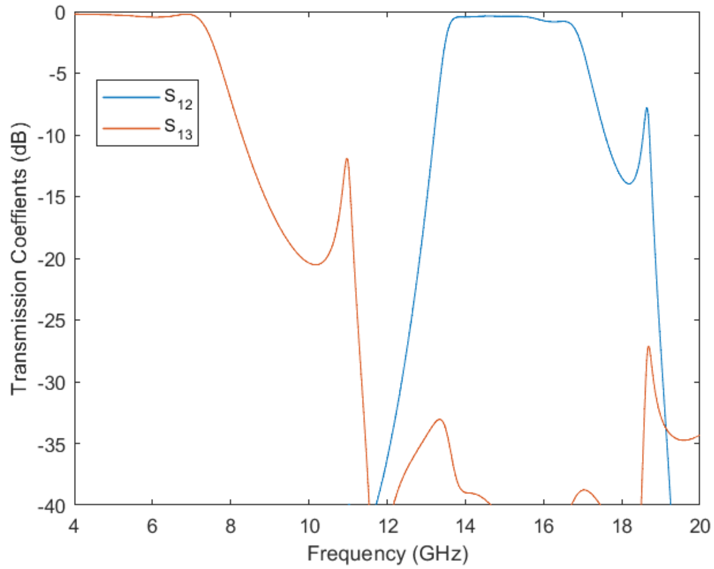


(a)

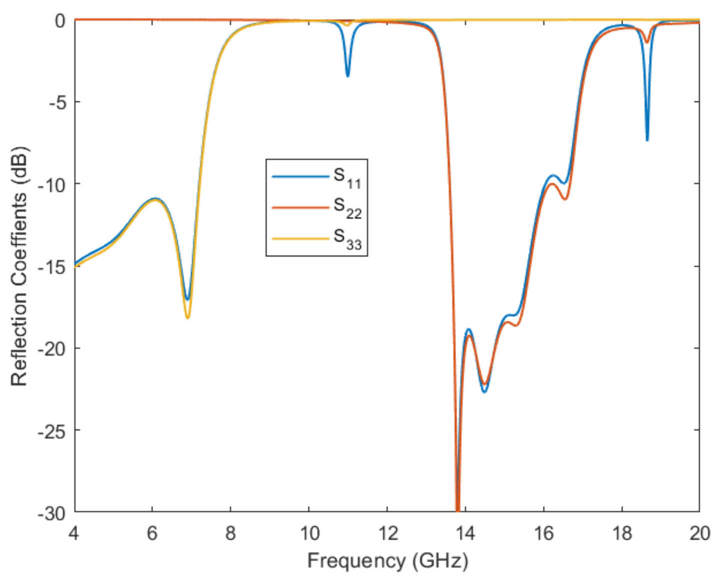


(b)

**Figure 18:** S-parameters of diplexer (a) Transmission coefficients, (b) Reflection coefficients

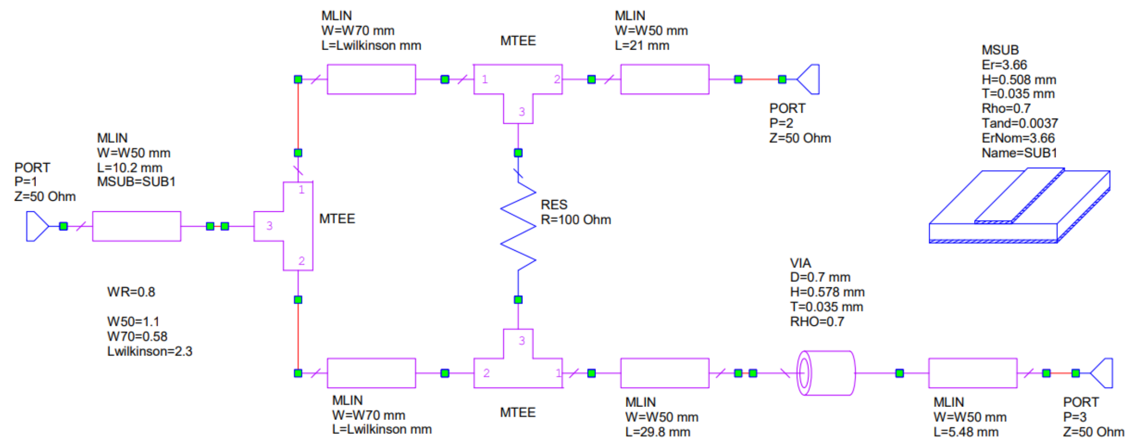


**Figure 19:** Schematic of Wilkinson power divider

### 2.3.2 A Wilkinson Power Divider

From [13], it is commonly known that a lossy three-port network can be designed having all ports matched with isolation between output ports. The Wilkinson power divider is a lossless network when the output ports are matched: that is, only reflected power from the output port is dissipated. WPD is proposed which divides the incoming signal into two way equal amplitude and same phase signals. It relies on $\lambda/4$ transformers to match the split ports to the common port. Since each end of the isolation resistor between ports 2 and 3 is at the same potential, no current flows through it and therefore the resistor is decoupled from the input signal. The schematic of power divider is depicted in Figure 19.

### 2.3.3 The Combination of Diplexer and WPD

In order to achieve dual-band operation with different polarization requirements, proposed feeding network is shown in Figure 21. It can be seen that the $3^{rd}$ port of Wilkinson power divider (which is presented in Figure 19) is connected through the via to one port of the diplexer which operated for upper frequency range.

Edge-coupled BPF is also constructed for Ku- band operation and transmission

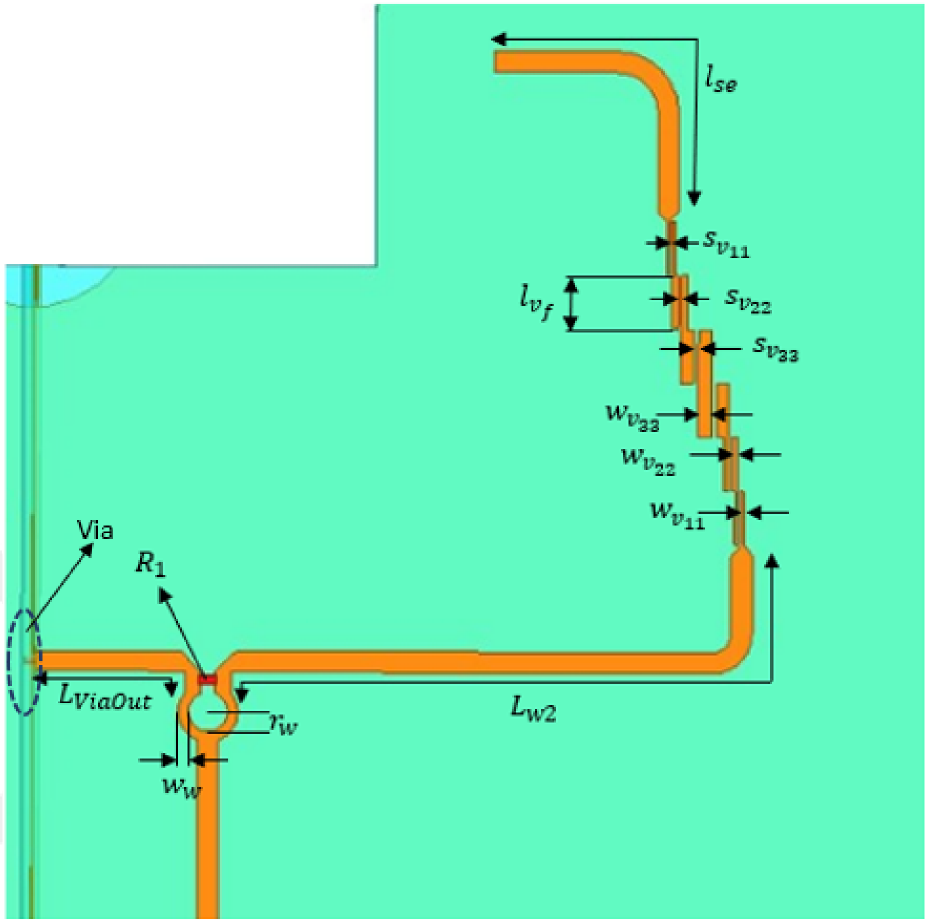


**Figure 20:** The combination of WPD, BPF, and Tline Phase Shifter

line phase shifter on the $2^{nd}$ port of power divider to achieve $90^o$ phase difference with equal magnitude of port 3 at upper frequency range.

Figure 20 which is captured from electromagnetic simulator depicts the combination of WPD, edge-coupled BPF, and transmission line phase shifter. Also, the metalized via is used to connect the microstrip trace of diplexer on orthogonal element that has to be cut off at the center line, as shown in Figure 20. Only the used area is shown for clarity.

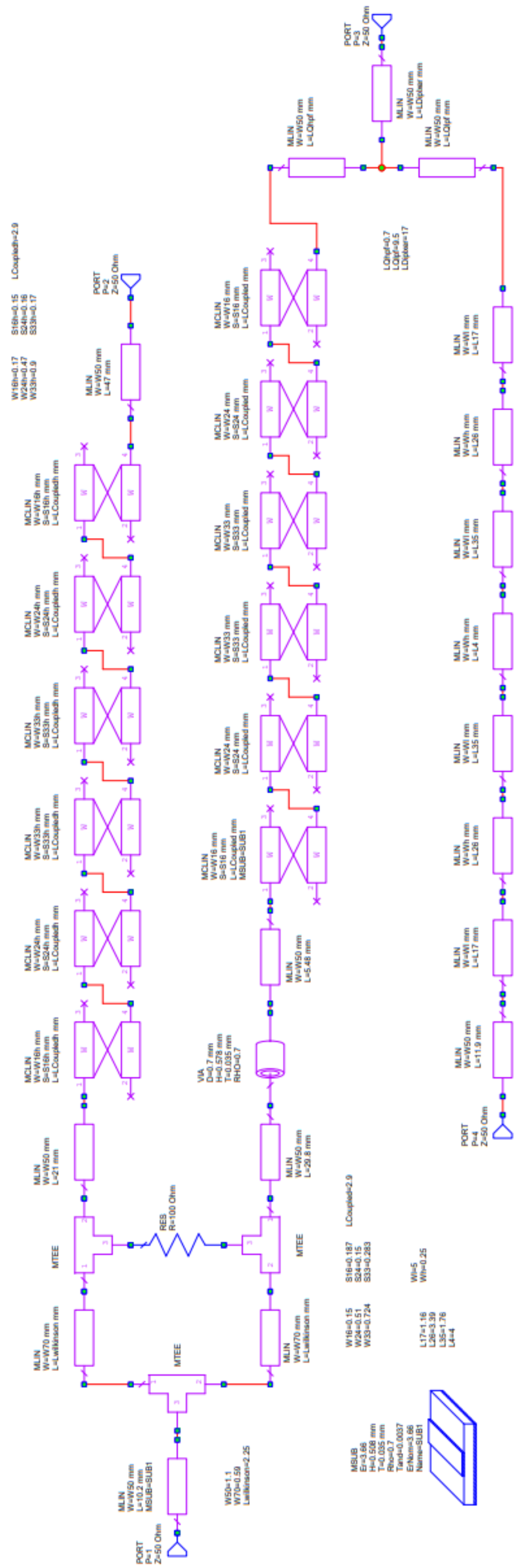

**Figure 21:** Schematic of Feed Network

# CHAPTER III

# SIMULATED AND MEASURED RESULTS

Based on our presented solution, two Vivaldi antennas are orthogonally located for compact consideration and are driven by a novel feeding structure design. Our dual-polarized antenna is employed by joining the radiators and feeding structure in a right way. Figure 22 depicts the configuration of the designed dual-polarized Vivaldi antenna. Rogers Corporation RO4350B [27] substrate with a thickness of 0.508 mm, dielectric constant of 3.66 and tangent loss of 0.0037 is used for the proposed antenna. In our study, the High Frequency Structure Simulator (HFSS) [28] is used for simulation.

## *3.1 Parts of Antenna Model*

In this section, simulation analysis of orthogonally placed two antenna and feeding structure is proposed.

### 3.1.1 Radiating Structure Simulation

The two elements are orthogonally placed as shown in Figure 23. These elements are almost identical, except the position of the microstrip-to-slotline transition points. To avoid overlaping of the two transition points of the elements, a small shift between them is proposed on vertical axes.

To observe the performance of Crossed Vivaldi antenna structure, simulation results are presented. The S-parameters of the crossed antenna are illustrated in Figure 24, and it can be seen that the reflection coefficients has -15 dB over much of both frequency bands. The isolation between two ports is better than -30 dB over the operating bands.

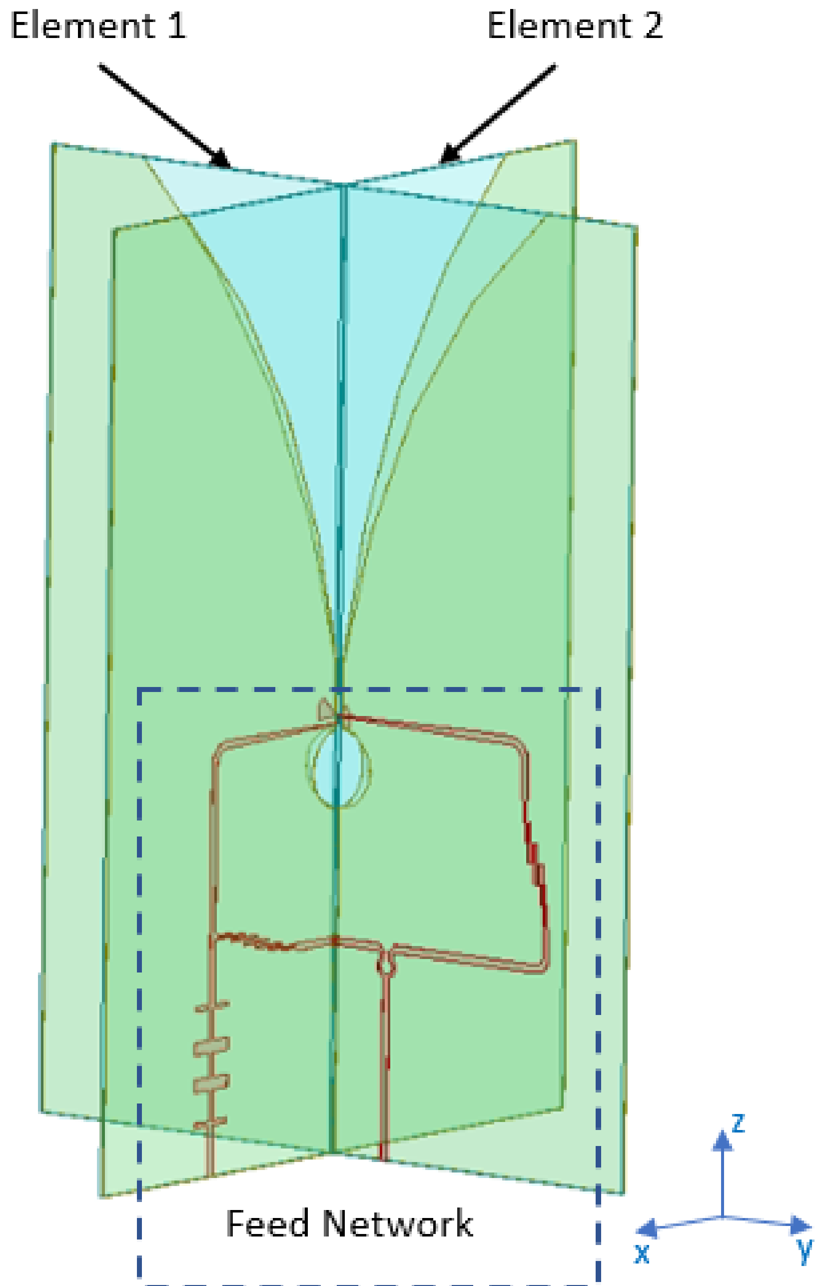


**Figure 22:** The proposed dual-polarized Vivaldi antenna

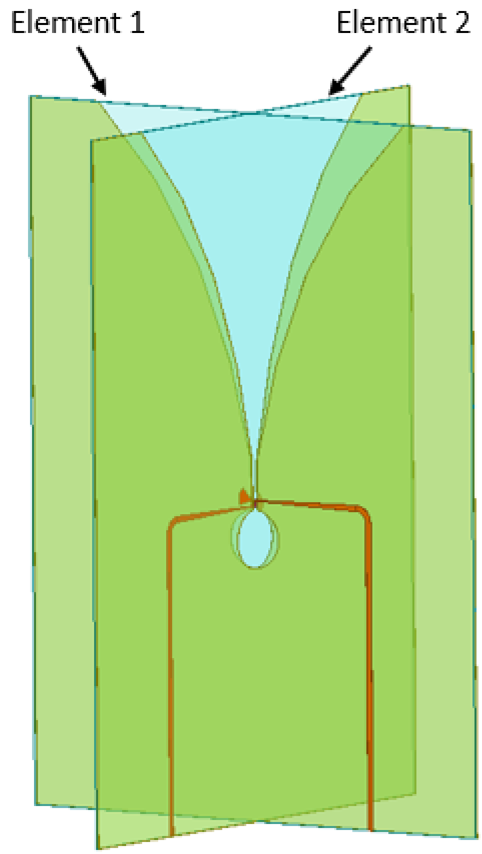


**Figure 23:** Crossed antenna structure

Figure 25 offers the simulated radiation patterns of the crossed antenna at 4 GHz, 5 GHz, 6 GHz, 14 GHz, 15 GHz, and 16 GHz for element 1 and element 2, respectively. It can be observed that simulated radiation patterns of each antenna are symmetrical over much of the both frequency bands, but there is a minor distortion of the main beam at upper frequency range. This is due to slight asymmetry of the structure.

The realized gain of the crossed antenna in the both operating frequency bands exhibits gain between 8.2 to 10.37 dBi for both antenna elements. The simulated efficiency is better than 0.9 in pass-band in C- and Ku- bands.

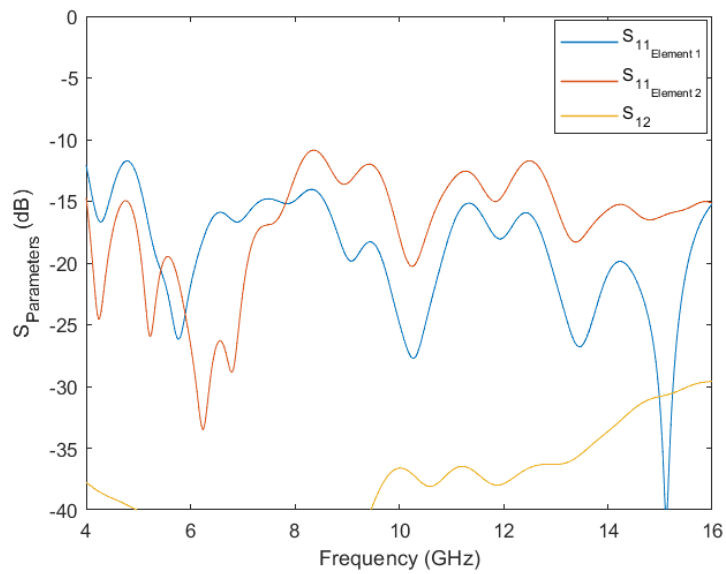


**Figure 24:** Simulated S-parameters of the crossed antenna structure

### 3.1.2 Feed Network Simulation

To make most of the antenna space, the feeding structure is integrated with the unexploited area of Vivaldi elements as shown in Figure 26. Thus, no extra space is needed, which also makes our Vivaldi to be easily constructed. Feed network is integrated with two orthogonally located substrates as shown in Figure 26. It is specially designed to compensate the linear and circular polarization, and ensure a good radiation performance. In order to divide the input signal of antenna into two-way signals for C-, and Ku- bands, diplexer is used. The diplexer comprises a stepped-impedance low-pass filter and an edge-coupled bandpass filter. A wilkinson power divider and a transmission-line phase shifter are employed to realize $90^o$ phase difference to achieve circular polarization at the upper frequency band.

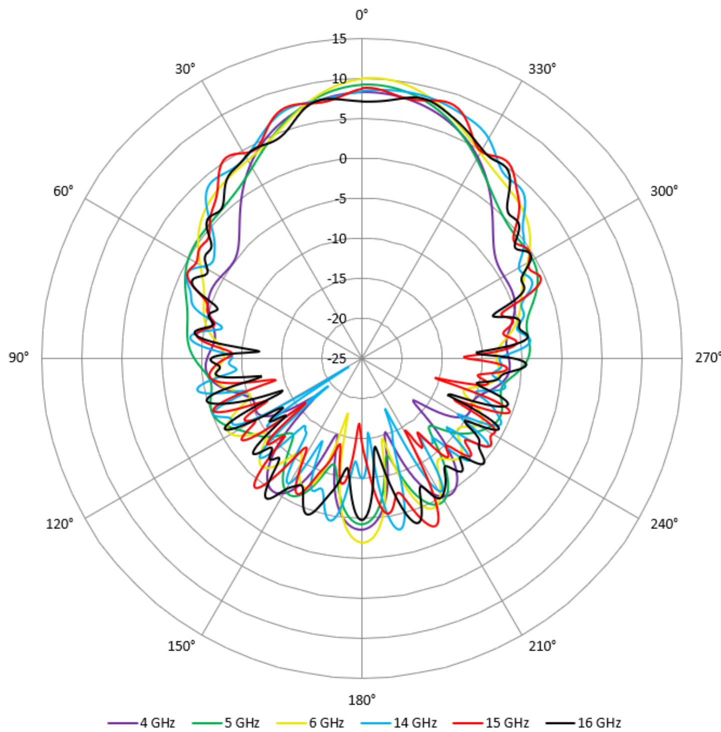


(a)

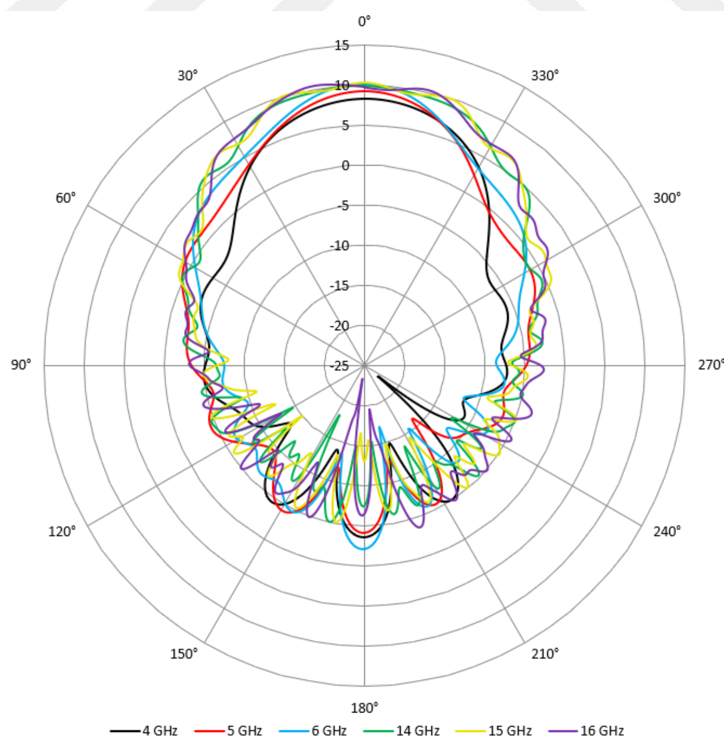


(b)

**Figure 25:** Simulated radiation pattern of the Crossed antenna structure at different frequencies (a) Element 1; (b) Element 2

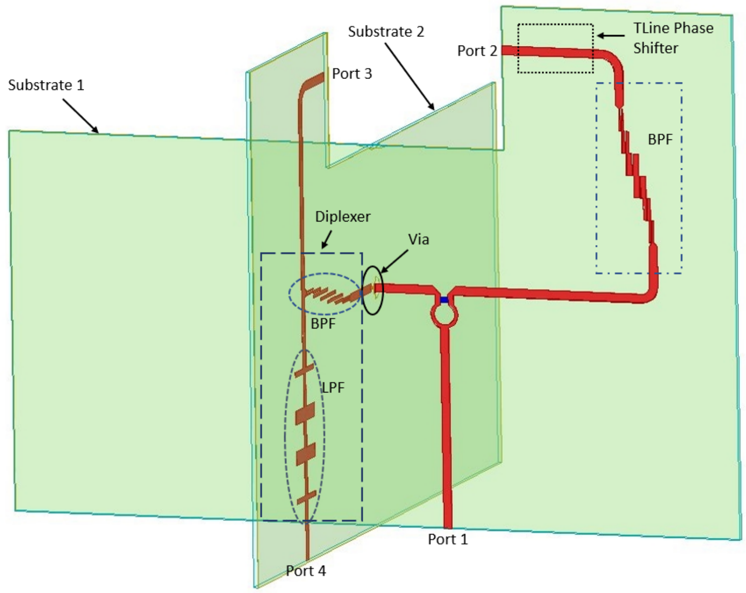


**Figure 26:** Structure of Feed Network

The simulations of feeding structure are offered in Figure 27. As evidinced in Figure 27 (b), reflection coefficients of feeding structure are better than -15 dB for most of the operation bands. It can be observed given in Figure 27 (a), there is tiny dissipated power because of substrate loss and resistor. The isolation is less than -30 dB and phase difference between port 2 and 3 is $90^o$ for upper band operation.

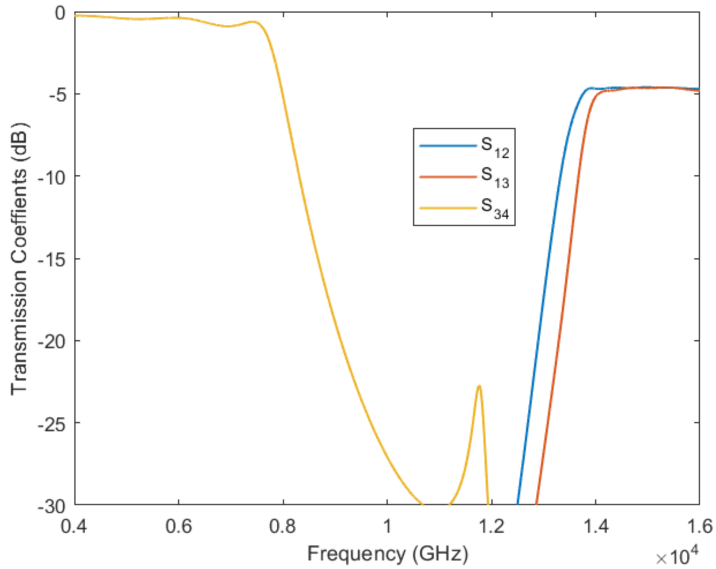


(a)

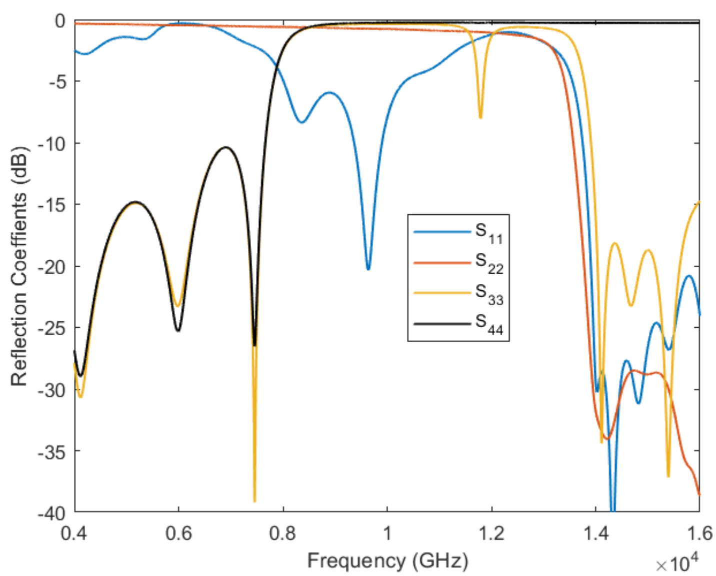


(b)

**Figure 27:** S-parameters of feeding structure (a) Transmission coefficients, (b) Reflection coefficients

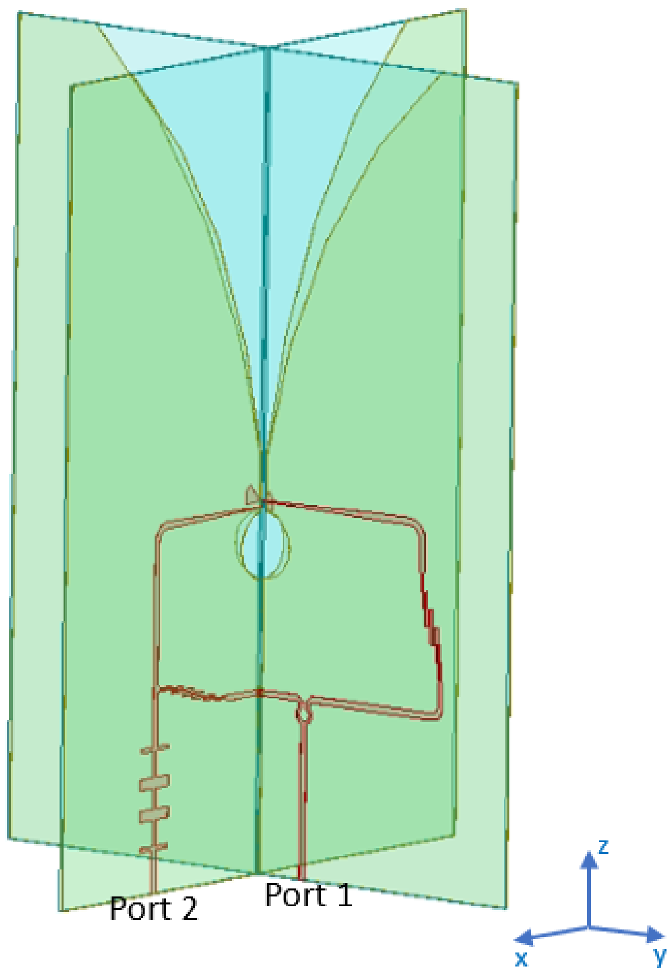


**Figure 28:** 3-D view of Vivaldi antenna operating in two frequency bands with distinct polarizations

## *3.2 Dual-Polarized Vivaldi Antenna*

Figure 28 presents the configuration and coordinate system of the proposed Vivaldi antenna operating in two frequency bands with distinct polarizations. It is simulated and the optimized parameters of the proposed antenna are shown in Table 2.

The simulated results of $S_{11}$ are presented in Figure 30 and the proposed Vivaldi antenna has -15 dB input reflections over much of both frequency bands.

**Table 2:** Dual-Polarized Vivaldi Antenna Parameters (units in millimeter). *The antenna is firstly designed for $h_{stub}$ is 0.578 mm. However, due to fabrication constraints, antenna design is adjusted to $h_{stub}$ is equal 1 mm

| | | | | | |
|---|---|---|---|---|---|
| $L_1$ | 65 | $l_{bpf}$ | 0.42 | $s_{v_{22}}$ | 0.15 |
| $W_1$ | 100 | $l_{hf}$ | 2.8 | $s_{v_{33}}$ | 0.24 |
| $l_{slot}$ | 9.13 | $L_{ViaIn}$ | 7.63 | $w_{v_{11}}$ | 0.15 |
| $w_{slot}$ | 1.35 | $l_p$ | 1.6 | $w_{v_{22}}$ | 0.31 |
| $R_{cavity}$ | 5.44 | $s_{h_{11}}$ | 0.195 | $w_{v_{33}}$ | 0.67 |
| $R_{stub}$ | 2.86 | $s_{h_{22}}$ | 0.172 | $r_w$ | 1 |
| $h_{stub}{}^*$ | 1 | $s_{h_{33}}$ | 0.375 | $w_w$ | 0.53 |
| $w_0$ | 0.15 | $w_{h_{11}}$ | 0.15 | $l_f$ | 22.9 |
| $w_f$ | 1.08 | $w_{h_{22}}$ | 0.34 | $Stub_{angle}$ | $70^\circ$ |
| $l_{diplexer}$ | 23.5 | $w_{h_{33}}$ | 0.413 | $R_1$ | 100 Ω |
| $l_{lpf}$ | 9.96 | $w_p$ | 1.5 | | |
| $l_{17}$ | 0.61 | $r_{Via}$ | 0.2 | | |
| $l_{26}$ | 4.26 | $l_{se}$ | 14.2 | | |
| $l_{35}$ | 1.71 | $l_{vf}$ | 2.8 | | |
| $l_4$ | 3.32 | $l_{w2}$ | 31.72 | | |
| $w_l$ | 7 | $L_{ViaOut}$ | 8.5 | | |
| $w_h$ | 0.81 | $s_{v_{11}}$ | 0.15 | | |

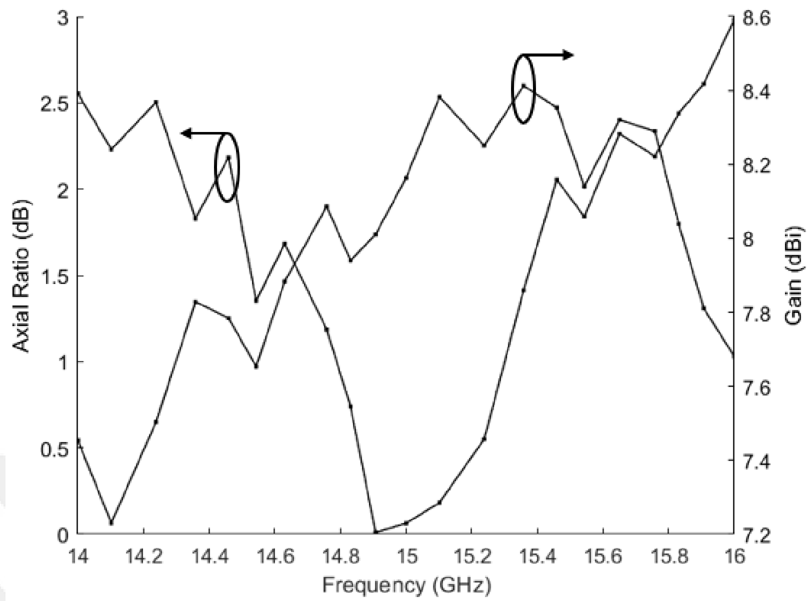


**Figure 29:** Simulated axial ratio and gain of the CP antenna

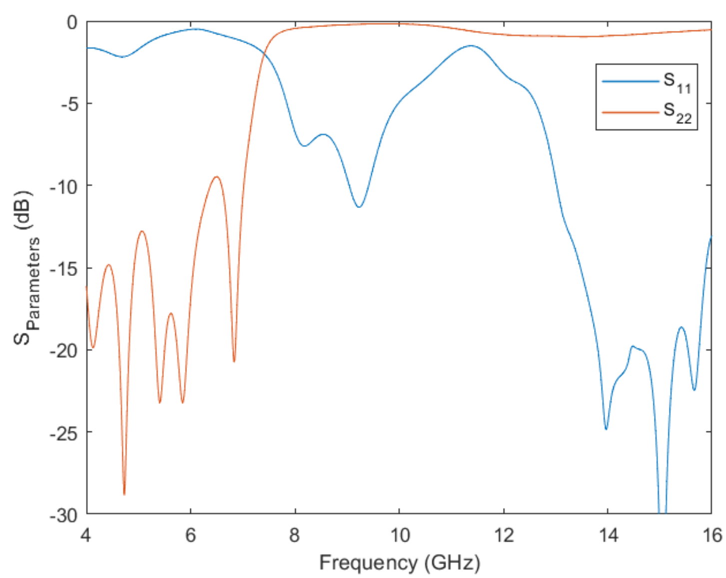


**Figure 30:** Simulated reflection coefficients of the proposed Vivaldi antenna operating in two frequency bands with distinct polarizations

### 3.2.1 Ku-Band CP Antenna Simulation

The propsed antenna is simulated and the results of port 1 as shown in Figure 28 are presented. The simulated axial ratio of Ku-band CP antenna shown in Figure 29 is corresponding to the phase difference is about to $90^o$ for upper frequency band. Consequently, the AR is below 2 dB in the operating bandwith. Figure 29 also depicts the IEEE gain of the CP antenna in the upper frequency range. The simulated gain is more than 7.2 dBi from 14 GHz, and the peak gain is about 8.6 dBi at 16 GHz. The simulated efficiency is better than 0.7 within AR bandwidth.

Figure 31 illustrates the simulated radiation patterns of the CP antenna at 14.35 GHz, 15 GHz, and 15.35 GHz in the xz- and yz-plane, respectively. It can be observed that simulated radiation patterns are almost symmetrical in the operating band. The minor distortion of the main beam is due to slight asymmetry of the structure but is deemed to be acceptable as a feed antenna for reflectors.

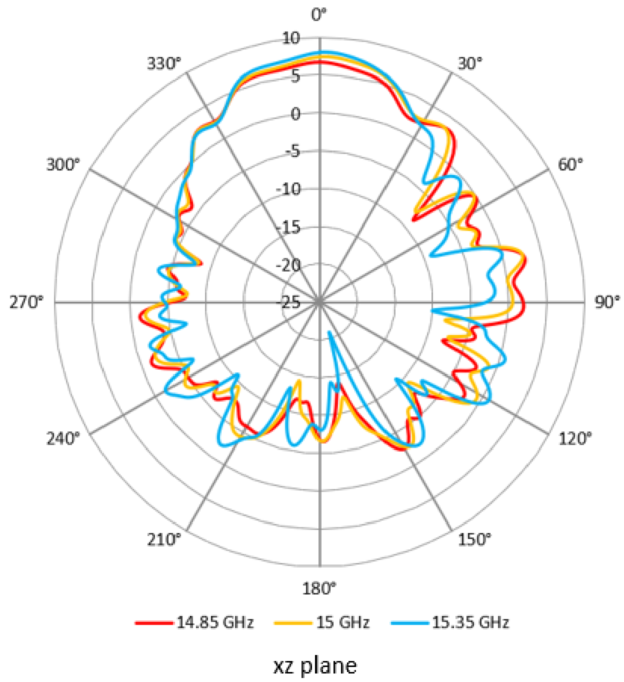


(a)

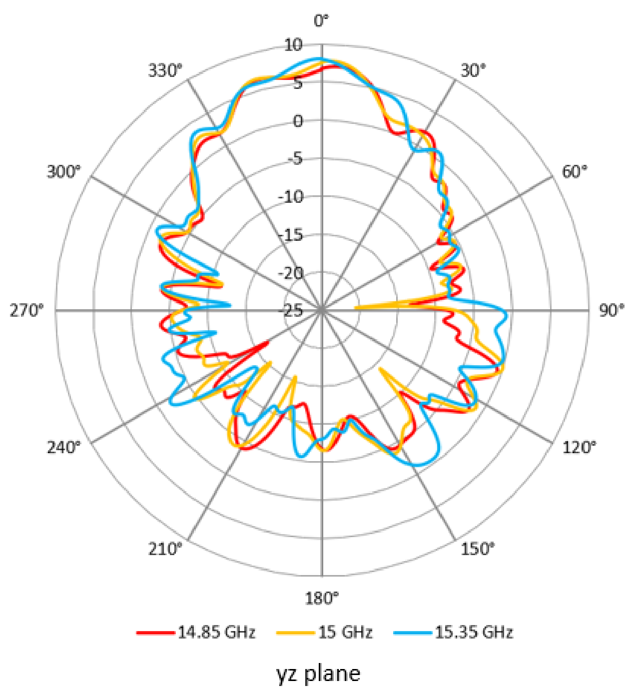


(b)

**Figure 31:** Simulated radiation pattern of the proposed CP antenna at 14.85, 15, 15.35 GHz (a) xz plane; (b) yz plane

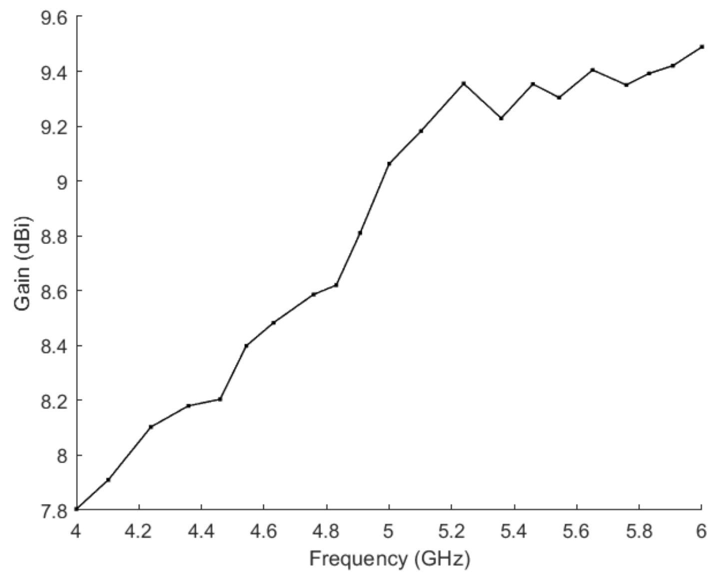


**Figure 32:** Simulated gain of LP antenna

### 3.2.2 C-Band LP Antenna Simulation

The offered antenna is simulated and the results of port 2 as shown in Figure 28 are presented. Figure 32 depicts the realized gain of the proposed LP antenna in the operating bandwith. The antenna exhibits gain between 7.8 to 9.5 dBi from 4 to 6 GHz. The simulated efficiency is better than 0.88 in passband.

Figure 33 presents the simulated radiation patterns of the LP antenna at 4 GHz, 5 GHz, and 6 GHz in the xz- and yz-plane, respectively. It can be seen that simulated radiation patterns are stable and symmetrical in the operating band. The beamwidth becomes a little broader with frequency increasing. The front-to-back ratio performance is also reasonably acceptable.

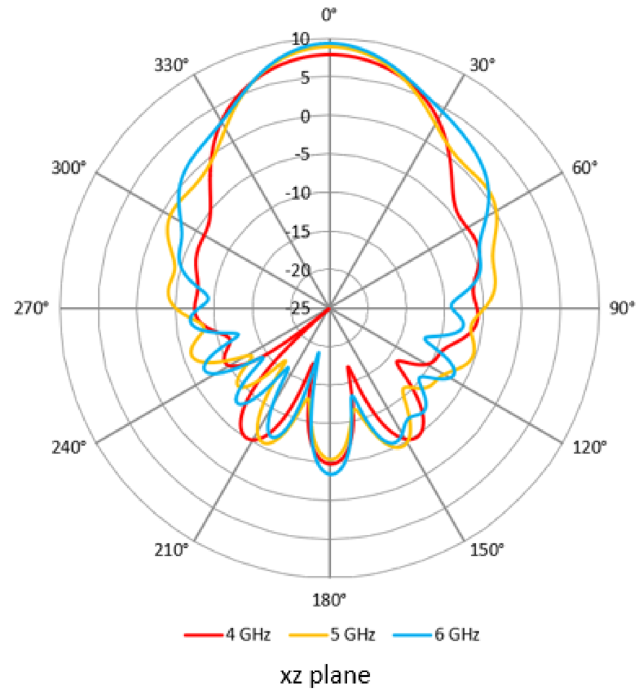


(a)

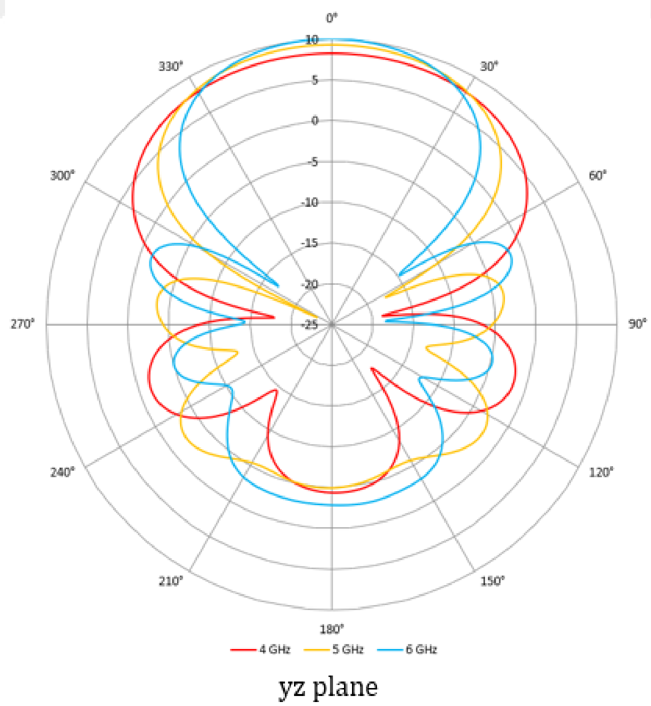


(b)

**Figure 33:** Simulated radiation pattern of the proposed LP antenna at 4, 5, 6 GHz (a) xz plane; (b) yz plane

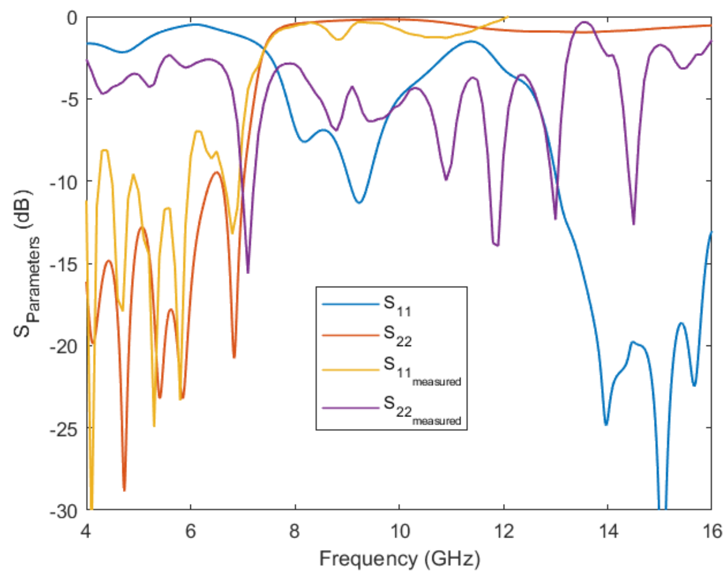


**Figure 34:** Simulated and measured input reflection coefficients of LP and CP antenna

## *3.3 Fabrication*

The fabricated dual-polarized antenna is presented in figure 21. In order to validate the design of Vivaldi antenna operating in two frequency range with different polariztions, a prototype has been fabricated. A basic model is also designed and used to hold the orthogonally placed two Vivaldi antennas, as shown in Figure 35.

The measured input reflection coefficient of LP antenna is reasonably acceptable for the initial prototype, but CP antenna does not work as presented in Figure 34. Radiation patterns and AR could be measured because of this fault. Possible problem comes from fabrication faults and can be named as;

- Via fault
- Short or open circuit in filter
- Ground problem (Cutting fault)

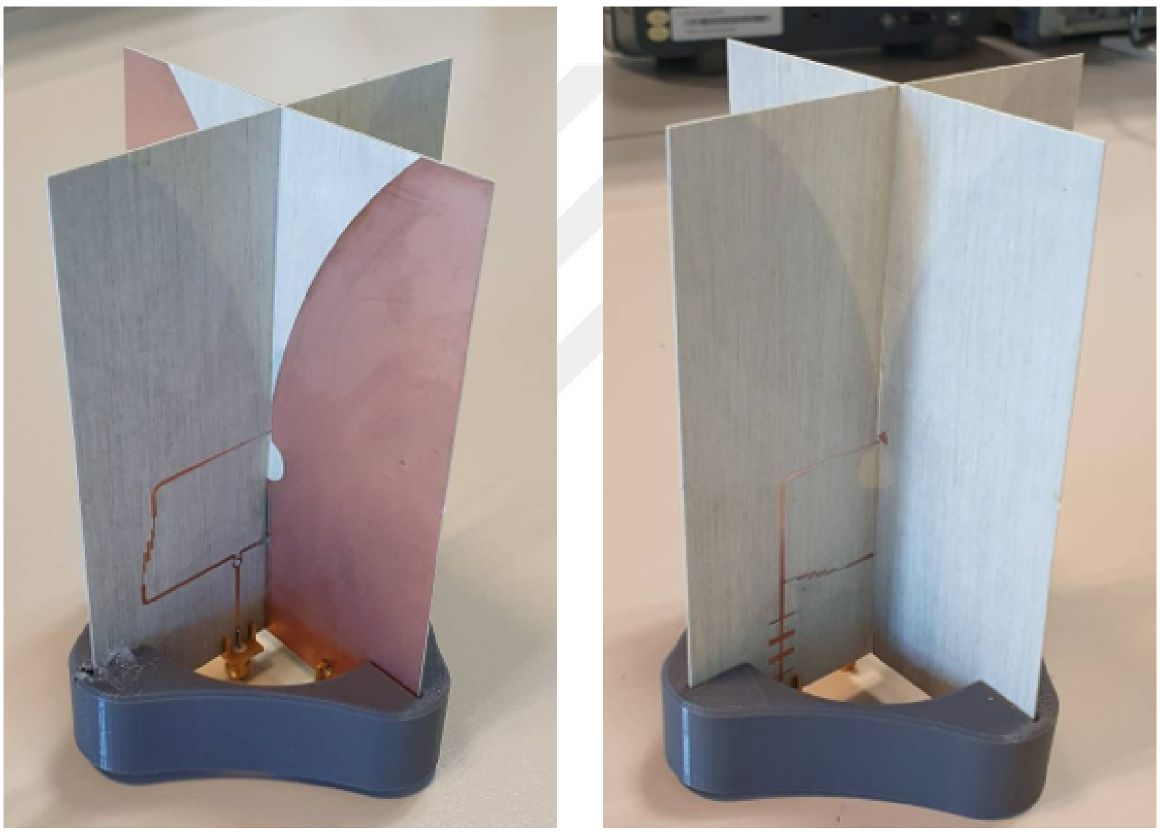

**Figure 35:** Photography of the fabricated dual-polarized Vivaldi antenna

# CHAPTER IV

# CONCLUSION

In this study, a cross-placed Vivaldi antenna with dual-polarization, stable and symmetrical radiation patterns and compact model has been proposed. The Vivaldi antenna are driven by a novel design of feeding network which splits incoming signal into two wherein one of them is linearly polarized between 4 and 6 GHz and the other one is circularly polarized from 14.5 to 15.5 GHz. Splitting of input signal into the two frequency bands, a diplexer is designed. A wilkinson power divider and a transmission-line phase shifter are employed to realize $90^o$ phase difference to achieve circular polarization at the upper frequency band. The feed network is integrated with the Vivaldi elements to ensure a compact form factor critical for reflector applications. In order to overlap of two microstrip feed lines, a small shift between them is introduced on vertical axes. This antenna is intended to be used as a feed antenna for reflector systems employed in radio link systems of drones. Combination of these distinct frequency bands with different polarization requirements allows use of single ground control antenna instead of two independent antennas thereby reducing cost and space requirements.

By correctly design and construct the feeding network and radiating elements, good impedance matching, which is better than -15 dB over much of the both frequency bands and AR better than 2 dB for circular polarization is obtained. In addition, the proposed dual-polarized antenna also exhibits gain between 7.2 to 9.5 dBi across the operating bands.

The dual-polarized Vivaldi antenna is partially measured. LP part has better than -10 dB input reflection, but CP part doesn't work because of fabrication faults.

Radiation pattern and AR measurement weren't carried out. The problems will be figured out and measurement will be completed in the short view.

# BIBLIOGRAPHY

[1] M. Sonkki, D. Sánchez-Escuderos, V. Hovinen, E. T. Salonen, and M. Ferrando-Bataller, "Wideband dual-polarized cross-shaped vivaldi antenna," *IEEE Transactions on Antennas and Propagation*, vol. 63, no. 6, pp. 2813–2819, 2015.

[2] P. J. Gibson, "The vivaldi aerial," *9th European Microwave Conference Proceedings, Sep. 1979*, p. 101–105, Sep. 1979.

[3] H. Schantz, *The Art and Science of Ultra-Wideband Antennas*. June 2015.

[4] Y.-W. Wang, G.-M. Wang, and B.-F. Zong, "Directivity improvement of vivaldi antenna using double-slot structure," *IEEE Antennas and Wireless Propagation Letters*, vol. 12, pp. 1380–1383, 2013.

[5] Y.-W. Wang, G.-M. Wang, and B.-F. Zong, "Directivity improvement of vivaldi antenna using double-slot structure," *IEEE Antennas and Wireless Propagation Letters*, vol. 12, pp. 1380–1383, 2013.

[6] Y. Liu, W. Zhou, S. Yang, W. Li, P. Li, and S. Yang, "A novel miniaturized vivaldi antenna using tapered slot edge with resonant cavity structure for ultrawideband applications," *IEEE Antennas and Wireless Propagation Letters*, vol. 15, pp. 1881–1884, 2016.

[7] J. Wu, Z. Zhao, Z. Nie, and Q.-H. Liu, "A printed uwb vivaldi antenna using stepped connection structure between slotline and tapered patches," *IEEE Antennas and Wireless Propagation Letters*, vol. 13, pp. 698–701, 2014.

[8] H. Feng, F. Zhang, and H. Zhang, "A dual polarized vivaldi antenna with the notched band by feed line filter on conductive plane," in *International Conference on Microwave and Millimeter Wave Technology (ICMMT)*, pp. 1–3, 2018.

[9] X. Li, Y. Li, J. T. Huang, and O. Yang Du, "A cross-slot loaded miniaturized uwb vivaldi dual-polarized antenna," in *International Conference on Microwave and Millimeter Wave Technology (ICMMT)*, pp. 1–3, 2021.

[10] X. Ren, S. Liao, and Q. Xue, "Design of wideband circularly polarized vivaldi antenna with stable radiation pattern," *IEEE Access*, vol. 6, pp. 637–644, 2018.

[11] X. Han, L. Juan, C. Changjuan, and Y. Lin, "Uwb dual-polarized vivaldi antenna with high gain," in *International Conference on Microwave and Millimeter Wave Technology (ICMMT)*, vol. 3, pp. 1–4, 2012.

[12] D.-H. Li, F.-S. Zhang, Y. Zhao, and L.-X. Cao, "Design of a miniaturized dual-polarized uwb vivaldi antenna," in *International Conference on Microwave and Millimeter Wave Technology (ICMMT)*, pp. 1–3, 2019.

[13] D. M. Pozar, *Microwave engineering.* 2005.

[14] S. A. Jadhav, S. B. Misal, A. Mishra, and A. Murugkar, "Designing of stepped impedance butterworth and chebyshev filters for wireless communication," in *IEEE Applied Electromagnetics Conference (AEMC)*, pp. 1–2, 2017.

[15] Z. B. Khan, Z. Huiling, G. Mehdi, and M. Y. Madni, "Design and measurement of cavity enclosed microstrip edge-coupled bandpass filter at ku band," in *IEEE International Conference on Signal Processing, Communications and Computing (ICSPCC)*, pp. 1–4, 2015.

[16] C. A. Balanis, *Antenna theory: analysis and design.* Wiley-Interscience, 2005.

[17] P. G. Frayne and A. J. Leggetter, "Wideband measurements on vivaldi travelling wave antennas," *IEE Colloquium on Multi-Octave Microwave Circuits, 1991*, pp. 5/1–5/6, 1991.

[18] J. Noronha, T. Bielawa, C. Anderson, D. Sweeney, S. Licul, and W. Davis, "Designing antennas for uwb systems," *Microwaves and Rf*, vol. 42, pp. 53–61, June 2003.

[19] K. Yngvesson, T. Korzeniowski, Y.-S. Kim, E. Kollberg, and J. Johansson, "The tapered slot antenna-a new integrated element for millimeter-wave applications," *IEEE Transactions on Microwave Theory and Techniques*, vol. 37, no. 2, pp. 365–374, 1989.

[20] M. Greenberg, K. Virga, and C. Hammond, "Performance characteristics of the dual exponentially tapered slot antenna (detsa) for wireless communications applications," *IEEE Transactions on Vehicular Technology*, vol. 52, no. 2, pp. 305–312, 2003.

[21] C. Granet, "Profile options for feed horn design," in *Asia-Pacific Microwave Conference. Proceedings*, pp. 1448–1451, 2000.

[22] M. M. I. Liton Chandra Paul, "A super wideband directional compact vivaldi antenna for lower 5g and satellite applications," *International Journal of Antennas and Propagation*, vol. 2021, p. 12, 2021.

[23] B. Shuppert, "Microstrip/slotline transitions: modeling and experimental investigation," *IEEE Transactions on Microwave Theory and Techniques*, vol. 36, no. 8, pp. 1272–1282, 1988.

[24] J. Knorr, "Slot-line transitions," *IEEE Transactions on Microwave Theory and Techniques*, vol. 22, no. 5, pp. 548–554, 1974.

[25] J. H. Shafieha, J. Nourinia, and C. Ghobadi, "Probing the feed line parameters in vivaldi notch antennas," *Progress in Electromagnetics Research B*, vol. 1, pp. 237–252, 2008.

[26] "Awr is now cadence — awr software." https://www.awr.com (Feb 2019).

[27] Ipcb, "Rogers ro4350b pcb." https://www.ipcb.com/material/590.html.

[28] "Ansys hfss 3d high frequency simulation software." https://www.ansys.com (accessed: 18 July 2022).